HHS Public Access

Author manuscript

J Control Release. Author manuscript; available in PMC 2019 August 10.

Published in final edited form as:

J Control Release. 2018 August 10; 283: 175–189. doi:10.1016/j.jconrel.2018.06.003.

Effect of Mannose Targeting of Hydroxyl PAMAM Dendrimers on Cellular and Organ Biodistribution in a Neonatal Brain Injury Model

Anjali Sharma[1,§], **Joshua E Porterfield**[1,2,§], **Elizabeth Smith**[1,3], **Rishi Sharma**[1], **Sujatha Kannan**[1,3,4,5], and **Rangaramanujam M. Kannan**[*,1,2,4,5]

[1]Center for Nanomedicine, Department of Ophthalmology, Wilmer Eye Institute Johns Hopkins University School of Medicine, Baltimore, MD 21231, USA

[2]Department of Chemical and Biomolecular Engineering, Johns Hopkins University, Baltimore MD, 21218, USA

[3]Department of Anesthesiology and Critical Care Medicine, Johns Hopkins University School of Medicine, Baltimore, MD 21287, USA

[4]Hugo W. Moser Research Institute at Kennedy Krieger, Inc., Baltimore MD, 21205, USA

[5]Kennedy Krieger Institute – Johns Hopkins University for Cerebral Palsy Research Excellence, Baltimore, MD 21218, USA

Abstract

Neurotherapeutics for the treatment of central nervous system (CNS) disorders must overcome challenges relating to the blood-brain barrier (BBB), brain tissue penetration, and the targeting of specific cells. Neuroinflammation mediated by activated microglia is a major hallmark of several neurological disorders, making these cells a desirable therapeutic target. Building on the promise of hydroxyl-terminated generation four polyamidoamine (PAMAM) dendrimers (D4-OH) for penetrating the injured BBB and targeting activated glia, we explored if conjugation of targeting ligands would enhance and modify brain and organ uptake. Since mannose receptors [cluster of differentiation (CD) 206] are typically over-expressed on injured microglia, we conjugated mannose to the surface of multifunctional D4-OH using highly efficient, atom-economical, and orthogonal Cu(I)-catalyzed alkyne–azide cycloaddition (CuAAC) click chemistry and evaluated the effect of mannose conjugation on the specific cell uptake of targeted and non-targeted dendrimers both *in vitro* and *in vivo*. *In vitro* results indicate that the conjugation of mannose as a targeting ligand significantly changes the mechanism of dendrimer internalization, giving mannosylated dendrimer a preference for mannose receptor-mediated endocytosis as opposed to non-specific fluid phase endocytosis. We further investigated the brain uptake and biodistribution

[*]Corresponding author: Rangaramanujam M. Kannan, Arnall Patz Distinguished Professor of Ophthalmology, Center for Nanomedicine at the Wilmer Eye Institute, 400 North Broadway, Baltimore, Maryland 21231, USA, Tel.: +1 443-287-8634; Fax: +1 443-287-8635; krangar1@jhmi.edu.

[§]These authors contributed equally

of targeted and non-targeted fluorescently labeled dendrimers in a maternal intrauterine inflammation-induced cerebral palsy (CP) rabbit model using quantification methods based on fluorescence spectroscopy and confocal microscopy. We found that the conjugation of mannose modified the distribution of D4-OH throughout the body in this neonatal rabbit CP model without lowering the amount of dendrimer delivered to injured glia in the brain, even though significantly higher glial uptake was not observed in this model. Mannose conjugation to the dendrimer modifies the dendrimer's interaction with cells, but does not minimize its inherent inflammation-targeting abilities.

Graphical abstract

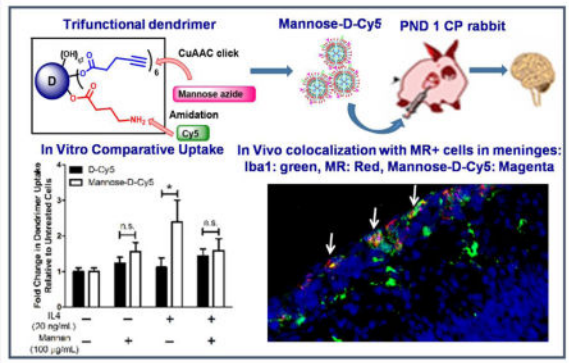

Keywords

Dendrimer; nanoparticle; targeting; mannose receptors; CD206; neuroinflammation; activated glia; cerebral palsy

1. Introduction

The central nervous system (CNS) is a highly sophisticated and complex system by design, posing formidable challenges for drug and gene delivery to treat CNS disorders. One of the major challenges in treating CNS disorders is the poor transport of many potentially therapeutic molecules across the blood brain barrier (BBB).[1–4] The discovery of novel drug delivery approaches that cross the BBB, penetrate brain tissue, and target injured regions within the brain is critical. Activated microglia-mediated neuroinflammation is a major hallmark of various neurological diseases making it a potential therapeutic target for drug delivery. In this regard, dendrimer based nanomedicine to target neuroinflammation for the delivery of drugs and imaging agents to specific cells in the brain has shown immense potential toward the treatment of neurological disorders.[5–7]

Amongst the multitude of nanoparticles being evaluated for biomedical applications, dendrimers stand out as a well-defined, hyperbranched, monodisperse, highly flexible and easily tunable nano-platform.[8–12] Owing to their commercial availability, water solubility, and relatively high biocompatibility, polyamidoamine (PAMAM) dendrimers have been widely explored for their potential in drug and gene delivery.[13–16] Hydroxyl-terminated PAMAM dendrimers (D-OH) specifically have been shown to be non-toxic, to have a low

immunogenicity, and to not activate the complement system.[17] Our group has reported that generation 4 D-OH (D4-OH) without any targeting ligand can cross the impaired BBB and selectively target activated microglia and astrocytes in multiple small and large animal models of neuroinflammation associated with the brain and retina upon systemic administration[18–20]. These models include a rabbit model of cerebral palsy (CP)[18], a rat model of retinal degeneration[21], a mouse model of neonatal stroke,[22] a canine model of hypothermic circulatory arrest induced brain injury,[23] and a primate model of ischemic optic neuropathy.[24] Towards our goal for improved targeting of neuroinflammation with this dendrimer platform, we envisioned that the anchoring of specific ligands, which can target receptors on injured microglia, might further enhance the glial uptake and retention of the dendrimer.

Mannose receptor [Cluster of Differentiation (CD) 206] is an endocytotic receptor found on macrophages and dendritic cells in the periphery as well as on microglia and astrocytes in the CNS.[25, 26] In many cases CD 206 is upregulated in response to inflammation [22, 27] and is one of several mechanisms of phagocytosis and endocytosis utilized by immune cells. [28–30] When mannosylated enzymes are bound to the receptor, the ligand is phagocytosed or endocytosed and transferred to lysosomes to be broken down. This mechanism is a property of the anti-inflammatory process that occurs after the cause of inflammation is addressed during the pro-inflammatory response. Since we have extensively studied the remarkable potential of PAMAM dendrimers for the targeted delivery of antioxidant and anti-inflammatories in maternal uterine inflammation-induced cerebral palsy (CP) rabbit model, we chose to study the effect of targeting mannose receptors in this CP model. CP can result from various traumas and stressors pre- or perinatally however as of late, there are few therapeutic options to decrease the severity of CP. Using this rabbit model, we have ascertained that chronic inflammation in this model of CP is critically related to the severity of the CP phenotype. Hydroxyl PAMAM dendrimers have ‘intrinsic’ specificity for activated microglia and macrophages in this CP model,[18, 22] we postulated that the addition of mannose[31] as a targeting ligand would facilitate increased uptake into the activated microglia and macrophages responsible for neuroinflammation.

We here present the synthesis of mannose-conjugated cyanine 5 (Cy5)-labeled G4 PAMAM dendrimers using click chemistry. Click chemistry is one versatile tool with shown applications in a variety of fields in chemistry including drug discovery, material science and polymer and dendrimer synthesis.[32–34] It has revealed itself brilliantly in the synthesis of backbones of dendrimers and dendrons, decoration and functionalization of dendrimer periphery, and conjugation of various bioactive ligands on the dendrimer surface.[35–38] Among various click reactions, the regioselective Cu(I)-catalyzed azide–alkyne [1, 3]-dipolar Huisgen cycloaddition (CuAAC) is seen as a major breakthrough in biomaterials synthesis in the past decade.[39, 40] We used a combination of CuAAC and esterification reaction to convert the monofunctional D4-OH surface to trifunctional to attach mannose as a targeting ligand and Cy5 as a fluorophore while still keeping enough hydroxyl groups intact as to not interfere with the dendrimer’s transport properties. We first investigated the ability of cells to engulf fluorescently-labeled targeted dendrimer (Mannose-D-Cy5) *in vitro* against non-targeted dendrimer (D-Cy5) in cells with and without CD206 overexpression and the quenching of mannose receptor by mannan. We further evaluated the biodistribution

of Mannose-D-Cy5 as compared to D-Cy5 in a neonatal rabbit model of CP. This study involves the most in depth investigation so far of both the local and global biodistribution of dendrimer in this neonatal rabbit model of CP including microdissection of the cortex, hippocampus, and periventricular region, and the observed localization of dendrimer in cells other than macrophages and microglia in the brain. In addition to brain, the uptake of dendrimers is also assessed in all other major organs including heart, liver, lungs, kidneys, spleen, and plasma using quantification methods based on fluorescence spectroscopy and confocal microscopy. These findings will contribute the better design and delivery of nanotherapeutics and imaging agents for diseases mediated by neuroinflammation.

2. Materials and Methods

2.1 Materials and reagents for intermediates and dendrimer synthesis

All reagents were used as supplied without prior purification unless otherwise stated. Hydroxyl-terminated, ethylenediamine core, generation-four polyamidoamine (PAMAM) dendrimer (D4-OH; diagnostic grade; 64 hydroxyl end-groups) was purchased from Dendritech Inc. (Midland, MI, USA). As received dendrimer was purified before use. Methanol was removed under reduced pressure to yield viscous oil. D4-OH dendrimer was re-dissolved in DI water and transferred to 3000 MWCO dialysis membrane and dialysed against 4 gallons of Nanopure water for 36 hours. The solution was stirred during dialysis, and water was changed 6-7 times at regular intervals. Purified dendrimer was lyophilized and dried to give hygroscopic white sticky material. Dendrimer was stored at −20°C under argon atmosphere. D-Mannose (99%), pyridine, acetic anhydride, boron trifluoride diethyl etherate, sodium methoxide solution, *N*-(3-Dimethylaminopropyl)-*N*′-ethylcarbodiimide hydrochloride(EDC), 4-(dimethylamino)pyridine (DMAP), *N*, *N*′-diisopropylethylamine (DIPEA), trifluoroacetic acid (TFA), 4-pentynoic acid, γ-(Boc-amino)butyric acid (BOC-GABA-OH), copper sulphate pentahydrate, sodium ascorbate, anhydrous dichloromethane (DCM), anhydrous tetrahydrofuran (THF), and anhydrous dimethylformamide (DMF) were purchased from Sigma-Aldrich (St. Louis, MO, USA). Cy5-mono-NHS ester was purchased from Amersham Biosciences-GE Healthcare. All other ACS grade solvents were from Fisher Scientific (Waltham, MA, USA). Dialysis membrane (MW cut-off 1000 Da) was obtained from Spectrum Laboratories Inc. (Rancho Dominguez, CA, USA). Deuterated solvents dimethylsulfoxide (DMSO-d6), methanol (CD_3OD), water (D_2O) and chloroform ($CDCl_3$) were purchased from Cambridge Isotope Laboratories, Inc. (Andover, Massachusetts).

2.2 Characterization of intermediates and dendrimers

2.2.1 Nuclear Magnetic Resonance (NMR)—NMR spectra were recorded on a Bruker 500MHz spectrometer at ambient temperatures. The chemical shifts in ppm are reported relative to tetramethylsilane as an internal standard for ^{1}H and $^{13}C\{^{1}H\}$NMR spectra. The resonance multiplicity in the ^{1}H NMR spectra are described as “s” (singlet), “d” (doublet), “t” (triplet), and “m” (multiplet) and broad resonances are indicated by “b”. Residual protic solvent of $CDCl_3$ (^{1}H, δ 7.27 ppm; ^{13}C, δ 77.0 ppm (central resonance of the triplet)), D_2O (^{1}H, δ4.79 ppm), and MeOD (^{1}H, δ3.31 ppm and ^{13}C, δ 49.0 ppm) were used for chemical shifts calibration.

2.2.2 High Performance Liquid Chromatography (HPLC)—The purities of intermediates and final dendrimer conjugate were analyzed using HPLC (Waters Corporation, Milford, Massachusetts) equipped with a 1525 binary pump, an In-Line degasser AF, a 717 plus autosampler, a 2998 photodiode array detector, and a 2475 multi λ fluorescence detector interfaced with Waters Empower software. A Symmetry C18 reverse phase column (Tosoh, Japan) having 5 μm particle size, 25 cm length, and 4.6 mm internal diameter was used. The HPLC chromatograms of the starting dendrimer (D4-OH) and all the intermediates were monitored at 210 nm and the final fluorescently labeled Mannose-D-Cy5 was monitored at both 650 and 210 nm using PDA and fluorescence detectors. A gradient flow was used in HPLC starting with 100:0 (H_2O/ACN), gradually increasing to 90:10 (H_2O/CAN) in 10 min, to 50:50 (H_2O/ACN) in 20 min and returning to 100:0 (H_2O/ACN) in 40 min maintaining a flow rate of 1 mL/min.

2.2.3 Mass spectroscopy—Accurate mass measurements (HRMS) were performed on Bruker microTOF-II mass spectrometer using ESI in positive mode and direct flow sample introduction in CH_3CN:H_2O (9:1) solvent system. Either protonated molecular ions $[M+nH]^{n+}$ or adducts $[M+nX]^{n+}$ (X = Na, K, NH_4) were used for empirical formula confirmation. MALDI-TOF experiments were performed on Bruker Daltonics MALDI instrument. The conjugate was dissolved in UPH water at 5 mg/ml and 2, 5-dihydroxybenzoic acid (DHB) matrix was dissolved in 50:50 (v/v) acetonitrile:water mixture at 10 mg/ml concentration. A sample was prepared by mixing 10 μL of conjugate solution with 10 μL of DHB solution and 3 μL of the sample was spotted on a Bruker Daltonics MALDI plate.

2.2.4 Dynamic light scattering (DLS) and Zeta potential (ζ)—The particle size and ζ-potential of D4-OH, and mannose conjugate were determined by dynamic light scattering (DLS) using a Zetasizer Nano ZS (Malvern Instrument Ltd. Worchester, U.K) equipped with a 50 mW He-Ne laser (633 nm). The conjugates (D4-OH and D4-mannose-NH_2 (**9**)) were dissolved in deionized water (18.2 Ω) to make solutions with a final concentration of 0.2 mg/mL. The solution was filtered through a cellulose acetate membrane (0.45 micron, PALL Life Science) and DLS measurements were performed in triplicate, at 25°C with a scattering angle of 173°.

2.3 Preparation of intermediates and final targeted dendrimer conjugate

All reactions were performed under dry conditions in an inert environment using distilled solvents. Reactions were monitored by analytical thin-layer chromatography (TLC) using silica gel 60 F254 pre-coated plates (E. Merck) and compounds were visualized with a 254 nm UV lamp, a mixture of iodine/silica gel and/or mixture of ceric ammonium molybdate solution (100 ml H_2SO_4, 900 ml H_2O, 25g $(NH_4)6Mo7O_{24}H_2O$, 10g $Ce(SO_4)_2$) and subsequent spots development by gentle warming with a heat-gun. Flash chromatography was performed using combiflash60.

Compounds **1** and **2** were synthesized following previously published procedures.[33, 41]

Synthesis of compound 3—To a stirred solution of peracetylated mannose **1** (715mg, 1.83mmoles) in anhydrous DCM (15 mL) at 0°C boron trifluoride diethyl etherate (1.2mL, 9.15mmoles) was added, followed by the addition of TEG mono tosylate **2** (1.113g, 3.66mmoles). The reaction mixture was stirred at room temperature (RT) for overnight. The completion of the reaction was monitored by TLC. Upon completion, the reaction was diluted with DCM. The organic layer was washed with sodium bicarbonate solution, water and brine. The organic layer was then dried over anhydrous sodium sulfate, filtered and evaporated under reduced pressure to afford crude compound 3. The column purification was performed on combiflash using ethyl acetate and hexanes as eluent; and the pure fractions were obtained in 40% ethyl acetate in hexanes. The pure fractions were evaporated to yield the product as viscous oil. Yield: 69%.

^{1}H NMR (500MHz, $CDCl_3$):δ 7.81 (d, J = 8.2 Hz, 2H), 7.35 (d, J = 8.0 Hz, 2H), 5.38 – 5.25 (m, 3H), 4.87 (s, 1H), 4.29 (dd, J = 12.2, 5.0 Hz, 1H), 4.18 (t, 2H), 4.14 – 3.99 (m, 2H), 3.85-3.77 (m, 1H), 3.71 (t, 2H), 3.69 – 3.62 (m, 3H), 3.60 (s, 4H), 2.46 (s, 3H), 2.16 (s, 3H), 2.10 (s, 3H), 2.05 (s, 3H), 2.00 (s, 3H).

^{13}C NMR:(126 MHz, $CDCl_3$) δ 171.08, 170.71, 170.07, 169.93, 169.73, 144.83, 133.02, 129.84, 128.00, 97.71, 72.47, 70.81, 70.75, 70.51, 70.33, 70.04, 69.57, 69.31, 69.23, 69.19, 69.09, 68.76, 68.73, 68.43, 67.38, 66.15, 63.55, 62.44, 61.78, 60.43, 21.67, 21.09, 20.99, 20.94, 20.80, 20.74, 20.73, and 14.23.

MS:m/z theoretical for $C_{27}H_{38}O_{15}S$, 634.19; found, 657.18 $[M + Na]^+$

Synthesis of compound 4—To a stirred solution of compound **3** (3g, 4.73mmoles) in anhydrous DMF, sodium azide (1.8g, 27.6mmoles) was added in portions and stirring was continued at RT for overnight. The completion of the reaction was monitored via TLC and upon completion; the reaction was diluted with water and extracted with ethyl acetate several times. The combined organic extracts were washed with water and brine to remove DMF. The organic layer was dried over anhydrous sodium sulfate, filtered and evaporated under reduced pressure. The residue was passed through the column using ethyl acetate and hexanes as eluent to afford compound **4** as viscous liquid. Yield: quantitative.

^{1}H NMR: (500 MHz, CDCl3) δ 5.36 (dd, J = 10.0, 3.5 Hz, 1H), 5.32 – 5.24 (m, 2H), 4.87 (d, J = 1.4 Hz, 1H), 4.29 (dd, J = 12.2, 5.0 Hz, 1H), 4.10 (dd, J = 12.2, 2.4 Hz, 1H), 4.06 (dd, J = 9.9, 5.0 Hz, 1H), 3.85 – 3.77 (m, 1H), 3.70-3.65 (m, 9H), 3.39 (t, 2H), 2.15 (s, 3H), 2.09 (s, 3H), 2.03 (s, 3H), and 1.98 (s, 3H).

^{13}C NMR:(126 MHz, $CDCl_3$) δ 170.72, 170.07, 169.93, 169.75, 97.75, 70.82, 70.72, 70.33, 70.09, 69.60, 69.10, 68.43, 67.44, 66.17, 62.44, 50.70, 20.94, 20.80, and 20.74.

MS:m/z theoretical for $C_{20}H_{31}N_3O_{12}$,505.19; found, 528.18 $[M + Na]^+$

Synthesis of compound 5—To a stirred solution of compound **4** (800mg, 1.58mmoles) in anhydrous MeOH (2mL) and anhydrous DCM (2mL) sodium methoxide solution (25w% in MeOH, 0.5 mL) was added dropwise to adjust the pH 9-10 and the reaction mixture was left for stirring overnight. The reaction pH was then adjusted with acidic resin to reach 6.

The resin was removed by filtration and the solvent was evaporated to yield a white solid. Yield: 90%.

^{1}H NMR: (500 MHz, D_2O) δ 4.91 (s, 1H), 3.98 (s, 1H), 3.90 (d, J = 11.7 Hz, 2H), 3.84 (s, 1H), 3.81-3.70 (m, 10H), 3.70-3.65 (m, 2H), and 3.52 (s, 2H).

^{13}C NMR: (126 MHz, D_2O) δ 99.92, 72.71, 70.46, 69.93, 69.60, 69.52, 69.48, 69.24, 69.17, 66.17, 66.37, 60.89, 60.35, and 50.12.

MS:m/z theoretical for $C_{12}H_{23}N_3O_{18,}$337.15; found, 360.14 $[M + Na]^+$

Synthesis of compound 6—To a stirred solution of D4-OH (274mg, 0.019mmoles) in DMF (6mL), 4-pentynoic acid (22.58mg, 0.228mmoles), EDC (54.63mg, 0.285mmoles), and DMAP (34.8mg, 54.63mmoles) were added, and stirring was continued at RT for 24 hours. The reaction mixture was then dialyzed against DMF for 12 H changing DMF after every 4 H followed by water dialysis for another 12 H changing water every 2 H. The aqueous solution was then lyophilized to yield white solid. Yield: 76%

^{1}H NMR: (500 MHz, DMSO-d_6) δ8.1-7.9 (m, CO-N*H*, G4-OH), 4.71 (bs, O*H*, G4-OH), 4.02 (m, G4-CH_2OCO), and 3.47–2.16 (m, aliphatic *H*, G4-OH; CH_2, pentyne linker; C*H* pentyne linker).

Synthesis of compound 7—To a stirring solution of compound **6** (551mg, 0.03mmoles) in DMF (6mL), BOC-GABA-OH (45.5mg, 0.223mmoles), EDC (57.3mg, 0.298mmoles), DMAP (36.5mg, 0.298mmoles) were added, and stirring was continued at RT for 24 hours. The reaction mixture was then dialyzed against water for 24 H changing water after every 4 H. The resulting aqueous solution was lyophilized to yield white solid. Yield: 72%

^{1}H NMR: (500 MHz, DMSO-d_6) δ8.1-7.7 (m, CO-N*H*, G4-OH), 4.70 (bs, O*H*, G4-OH), 4.05-3.97 (m, G4-CH_2OCO), 3.50–2.00 (m, aliphatic *H*, G4-OH; CH_2, both pentyne and GABA linkers; C*H* pentyne linker), 1.67-1.55 (m, CH_2 GABA linker), and 1.36 (bs, BOC *H*).

Synthesis of compound 8—To a stirred solution of compound **7** (458.04mg, 0.03mmoles) in dry DCM (4mL), TFA (3 mL) was added drop wise and stirring was continued for overnight at RT. The reaction mixture was diluted with methanol and evaporated on rotary evaporated. This process was repeated several times to remove traces of TFA. The residue was re-dissolved in anhydrous methanol and treated with A21 ion exchange resin to remove TFA salt. The resin was filtered off and the solvent was evaporated to afford compound **8** as off-white solid in quantitative yield.

^{1}H NMR: (500 MHz, DMSO-d_6) δ 8.7-8.15 (m, CO-N*H*, G4-OH), 7.89 (bs, NH_2), 4.45-4.35 (m, G4-CH_2OCO-pentyne linker), 4.10-3.90 (m, G4-CH_2OCO-GABA linker), 3.80–2.2 (m, aliphatic *H*, G4-OH; CH_2, pentyne and GABA linkers; C*H* pentyne linker), and 1.84-1.72 (m, CH_2 GABA linker).

Synthesis of compound 9—To a stirred solution of acetylene terminating dendrimer **8** (680mg, 0.046mmoles) and mannose azide **5** (150mg, 0.45mmoles) in a mixture of THF (2mL) and (2mL), a solution of $CuSO_4.5H_2O$ (7mg, 0.02mmoles) in distilled H_2O (1 mL) was added followed by the addition of sodium ascorbate (11mg, 0.06mmoles). The reaction was stirred at RT for 36 hours. The reaction mixture was dialyzed using 1000 cut off dialysis membrane against water for 24 H. Water was changed every 4 hours. The aqueous solution was then lyophilized to obtain the product as white solid.

^{1}H NMR: (500 MHz, DMSO-d_6) δ 8.3-7.8 (m, CO-N*H*, G4-OH and s, triazole *H*), 4.63 (bs, mannose *H*),4.47 (bs, mannose *H*), 4.05-3.97 (m, G4-CH_2OCO), 3.79 (bs, mannose *H*), 3.70-3.57 (m, mannose *H*), 3.55-3.44 (m, mannose TEG *H*), 3.43–2.00 (m, aliphatic *H*, G4-OH; and CH_2, both pentyne and GABA linkers), and 1.85-1.77 (m, CH_2GABA linker).

Synthesis of compound 10—To a stirred solution of compound **9** (150mg, 0.01mmoles) in DMF (3mL), DIPEA (0.1mL) was added, followed by the addition of Cy5 NHS ester (12mg, 0.02mmoles) dissolved in 1 mL DMF. The stirring was continued at RT for 12 H. The reaction mixture was dialyzed against DMF for 12 H, changing DMF every 4 H followed by the dialysis against H_2O for 8 H. The water was changed every 3 H. The aqueous solution was then lyophilized to afford compound 10 as blue solid in % yield.

^{1}H NMR: (500 MHz, DMSO-d_6) δ 8.40-8.30 (m, Ar*H* Cy5), 8.10-7.75 (m, CO-N*H*, G4-OH and s, triazole *H*), 7.70-7.64 (m, Ar*H*Cy5), 7.36-7.29 (m, Ar*H* Cy5), 6.85-6.83(m, Cy5 *H*), 6.67-6.54 (m, Cy5*H*), .35-6.35 (m, Cy5*H*), 5.80-5.76 (m, Cy5*H*), 4.71 (bs, G4-OH), 4.63 (bs, mannose *H*), 4.46 (bs, mannose *H*), 4.05-3.97 (m, G4-CH_2OCO), 3.79 (bs, mannose *H*), 3.70-3.57 (m, mannose *H*), 3.55-3.44 (m, mannose TEG *H*), 3.43–2.00 (m, aliphatic *H*, G4-OH; and CH_2, both pentyne and GABA linkers), 1.84-1.81 (m, CH_2 linker), 1.71-1.40 (m, -CH_2 Cy5), and 1.36-1.12 (m, -CH_2 Cy5).

MALDI-ToF: Theoretical: 17,583; found 17,581

2.4 Comparative in vitro analysis of dendrimer uptake due to mannose conjugation in murine macrophages

2.4.1 Cell culture—Murine macrophage cell line (RAW 264.7) was purchased from ATCC (Manassas, VA) and used for all studies published. Cells were cultured in 75cm^2 flasks in media consisting of 1x Dulbecco's Modified Eagle Medium (Fisher) with 10% FBS (Fisher) and 1% penicillin-streptomycin (Fisher). Cells were maintained in an incubator at 37°C and 5% CO_2 with media replacements every two days and passaging utilizing 0.05% trypsin-EDTA (Fisher) when cells reached 80% confluence.

2.4.2 Uptake studies—We performed comparative uptake studies as previously reported.[42] Cells utilized were between passages 6 and 15. Sub-confluent cells were obtained from a 75cm^2 flask with incubation 0.05% trypsin-EDTA followed by cell scraping. Cells were washed with and resuspended in fresh media. 6-well plates were then seeded with 3×10^5 cells each in duplicate and allowed two days to adhere and grow to 60-80% confluence. Cells were activated with LPS endotoxin (*Escherichia coli* serotype 127; B8: Sigma Aldrich, St Louis, MO) at a concentration of 100 ng/mL or exogenous interleukin 4 (IL-4)

(Peprotech, Rocky Hill, NJ) at a concentration of 20 ng/mL for three hours prior to treatment with dendrimer. CD 206 was blocked with mannan (*Saccharomyces cerevisiae*, Sigma) at a concentration of 100 μg/mL for 30 minutes prior to treatment with dendrimer. D-Cy5 and Mannose-D-Cy5 were applied to cells for a final concentration of 20 μg/mL and incubated with the cells for eight hours. Wells requiring LPS or Mannan were co-treated at 100 ng/mL and 100 μg/mL respectively.

After eight hours, media was removed and wells were washed twice with sterile dPBS. Cells were then incubated in 1 mL of 0.05% trypsin-EDTA, and well bottoms were scraped to remove all cells. Wells were washed and trypsin-EDTA was neutralized with an additional 3 mL of fresh media. After counting the cells, they were pelleted at 1400 rpm for 3 min, media was removed, and cells were resuspended in 200 μL of methanol, transferred to a sterile Eppendorf tube, and stored at −80°C.

2.4.3 Dendrimer extraction and fluorescence quantification—Cells in methanol underwent three freeze-thaw cycles in liquid nitrogen as well as 10 minutes of homogenization with a stainless steel bead on a Bullet Blender Storm 24 tissue homogenizer (Next Advantage Inc., Averill Park, NY) at power level 4. Homogenates were then centrifuged at 15000 rpm for 10 minutes at 4°C to pellet cell debris. The supernatants were analyzed for fluorescence intenstity of Cy5 (λ_{ex}=645 nm, λ_{em}=662 nm) on a RF5301PC spectrofluorophotometer running Pamorama3 software (Shimadzu Scientific Instruments, Columbia, MD) and adjusted for background fluorescence from untreated cells run in the same experiment. Dendrimer concentrations were then calculated based on previously created calibration curves for the specific batches of D-Cy5 and Mannose-D-Cy5 used.

2.4.4 Confocal Imaging of Uptake Studies—For confocal imaging cells were seeded at 5×10^5 cells per dish in 35mm glass bottom dishes coated in poly-d-lysine (MatTek Corporation, Ashland, MA, USA). Cells then were allowed to adhere and grow for two days before undergoing the same treatment scheme as in 2.4.2. After washing twice with sterile dPBS (5 min) dishes were incubated in 1 mL of cold 4% paraformaldehyde in dPBS at room temperature for 10 min. Wells were then washed once with DI water and incubated in 1 mL of cold 1:1 EtOH:Acetone for 5 min at room temperature. The EtOH:Acetone solution was then aspirated off and the dishes were allowed to dry at room temperature before storage at 4°C.

Prior to immunohistochemical staining, cells were rehydrated by incubation in TBS (Fisher) for 5 min before they underwent 4 hours of blocking and permeabilization in TBS with 0.1% Triton X (Sigma), 1% bovine serum albumin (BSA) (Fisher), and 5% normal goat serum (Fisher) at 4°C. After removing the blocking buffer, cells were incubated with rabbit polyclonal antibody to mouse mannose receptor (Abcam, Cambridge, UK) diluted 1:500 in TBS with 0.1% Triton X and 1% BSA at 4°C overnight. Cells were then washed with TBS with 0.1% Triton X three times for 5 min each at 4°C before incubation with AlexaFluor 488 goat anti-rabbit IgG (Life Technologies, Carlsbad, CA, USA) diluted 1:200 in TBS with 0.1% Triton X overnight at 4°C. Dishes were then washed two times for 5 min at 4°C with TBS with 0.1% Triton X and once for 5 min with TBS at 4°C. Cells were finally treated with NucBlue Fixed Cell Stain ReadyProbes Reagent (Life Technologies) for 10 min at 4°C

before a final set of three washes in TBS at 4°C. Cells were stored at 4°C until imaging. Glass-bottom dishes were then imaged on a Zeiss 710 confocal microscope (Zeiss, Oberkochen, Germany) running ZEN software (Zeiss). All laser settings were kept the same between images, and z-stacks were processed into maximum intensity projections.

2.4.5 CD206 Expression Analysis—Raw 264.7 cells underwent the full growth and treatment scheme explained in 2.4.2 in 6-well plates and were utilized between passages 8 and 15. After washing twice with sterile dPBS, cells incubated in 1 mL of Trizol (Life Technologies) and washed in the Trizol supernatant until the well bottom appeared devoid of cells. Trizol samples were then transferred to RNA-free 1.5 mL Eppendorf tubes and stored at −80°C.

RNA was extracted by first a phase separation through the addition of 0.2 mL of chloroform (Sigma) to each Trizol sample having been thawed on ice. After incubating at room temperature for 3 minutes, the samples were centrifuged at 12000 × *g* for 15 min at 4°C. The aqueous layer was then transferred to a new PCR-clean Eppendorf tube to which 0.5 mL of isopropanol (Sigma) was added to precipitate the RNA. Following a 10 minute incubation at room temperature, samples were centrifuged at 12000 × *g* for 10 min at 4°C, after which the supernatant was removed. The RNA pellets were then washed with 1 mL of 75% EtOH in DEPC water (Fisher) by brief vortexing before precipitating again via centrifugation at 7500 × *g* for 5 min at 4°C. The supernatant was removed and the pellets were allowed to air dry for 10 min after which the RNA was resuspended in 20 μL of DEPC water and analyzed for content and purity on a Nanodrop 2000 Spectrophotometer (Fisher). Any samples with AD260/AD280 values lower than 1.60 were discarded.

RNA samples were converted to cDNA with a high capacity cDNA reverse transcription kit (Applied Biosystems, Foster City, CA) and incubation on a T100 Thermal Cycler (Bio-Rad, Hercules, CA). cDNA was stored at −80°C until RT-qPCR. Samples were mixed with fast SYBER green master mix and either murine GAPDH [Forward: TGTCGTGGAGTCTACTGGTGTCTTC; Reverse: CGTGGTTCACACCCATCACAA] or murine CD206 [Forward: TCTTTGCCTTTCCCAGTCTCC; Reverse: TGACACCCAGCGGAATTTC] primers (Integrated DNA Technologies, Coralville, IA) in microAMP fast 96-well reaction plates (Applied Biosystems) and analyzed on a CFXConnectTM Real Time PCR machine (Bio-Rad). Amplification cycles were compared between samples with GAPDH expression levels as an internal standard via $2^{\Delta\Delta Ct}$ analysis. For each sample GAPDH and CD206 were run on the same plate.

2.5 Qualitative and Quantitative analyses of Mannose-D-Cy5 biodistribution in a neonatal rabbit model of cerebral palsy (CP)

2.5.1 Animals—Female New Zealand white rabbits (2.2-2.5 kg) were procured from Charles River (state, USA). All animals were housed at 22°C, 50% relative humidity and 12-h light/dark cycle. All protocols were approved by the Johns Hopkins University Animal Care and Use committee (ACUC).

2.5.2 Neonatal rabbit model of cerebral palsy—In accordance with previously published protocols[43–45] pregnant female rabbits were subjected to a laparotomy on the

28th day of gestation (G28). In this procedure, 3200 units of the endotoxin LPS (*Escherichia coli* serotype 127; B8: Sigma Aldrich, St Louis, MO) was injected into the uterine wall (distributed equally along uterus). Two days later on gestational day 30/PND 0, labor was induced using Pitocin® (JHP Pharmaceuticals; Rochester, MI). After delivery, newborn rabbit kits were given 1 ml of Lactated Ringers saline solution (Hospira; Baltimore, MD) and 1 ml of rabbit milk replacer (Wombaroo; South Australia, Australia). Kits were kept in incubators maintained at a temperature of 32-35°C and relative humidity of 50-60%.

2.5.3 PND 0 Injections—Both D-Mannose-Cy5 and D-Cy5 (55 mg/kg each; 200 μl injection volume) were injected intravenously (i.v.) on postnatal day 0 (PND0). At either 1, 4, or 24 hours post-injection, rabbit kits were euthanized with 200μL of euthasol delivered intraperitoneally, and perfused transcardially with 50mL of dPBS after a blood sample was drawn from the right atrium.

2.5.4 Dendrimer extraction and fluorescence quantification—Tissue samples were analyzed for biodistribution through homogenization and extraction as previously published in a blinded manner.[37] The brain was bisected; one hemisphere of each brain was preserved for microscopy in formalin for 48 hours and then increasing concentrations of sucrose solution (15%, 30%) for 24 hours each. The other hemisphere of the brain in addition to the heart, lungs, liver, kidneys, and spleen were frozen on dry ice and maintained at −80°C until processing. The blood sample was centrifuged in a heparin-coated tube (Sigma), and the plasma supernatant was removed and stored at −80C in a protein lo-bind Eppendorf tube (Sigma). At a later time the organs were thawed, massed, and dissected. Samples from each organ (3 from liver, lungs, kidneys; 2 from heart; 1 from spleen, cortex, hippocampus, and periventricular region) were homogenized in methanol in a 1mL:100mg tissue ratio with 0.9-2.0mm stainless steel homogenization beads on a Bullet Blender Storm 24 tissue homogenizer (Next Advantage Inc., Averill Park, NY) for 10 minutes at power level 6 for brain and spleen, and power level 12 for heart, liver, lungs, and kidneys. Homogenized samples were centrifuged at 15000 rpm for 10 minutes at 4°C, then the supernatant was transferred to a protein lo-bind Eppendorf tube and stored at −80°C. Plasma was diluted 10-fold in dPBS then passed through a 0.2 μm pore PES filter. Before measuring fluorescence intensity, HPLC analyses of supernatants were carried out to confirm the stability of the conjugates *in vivo*. The fluorescence intensity of Cy5 (λ_{ex}=645 nm, λ_{em}=662 nm) in each sample was determined with a RF5301PC spectrofluorophotometer running Pamorama3 software (Shimadzu) and adjusted for background fluorescence from healthy control tissue. The fluorescence intensity values were then converted to dendrimer concentrations through batch-specific calibration curves for D-Cy5 and Mannose-D-Cy5, upon unblinding of sample identifications.

2.5.5 IHC and imaging—Once sunk in 30% sucrose PBS, formalin-fixed brains were sectioned at 30μm using a cryostat and saved in six series. One series of slides was incubated in 3% Donkey serum (in 0.1% Triton PBS) for 30 min, then in goatanti-Iba1 (Abcam) and mouse anti-mannose receptor (Abcam) for 15-18 hours (1:500 in 0.1%Triton PBS) at 4°C. Once the incubation in primary antibodies was complete, the slides were washed with PBS (2× 2 min) and then incubated in Alexa Fluor 488 donkey anti-goatand Alexa Fluor 594

donkey anti-mouse (Fisher) and then incubated in DAPI for 15 min (1:1000 in PBS). After 2 more washes in PBS, slides were allowed to dry, and once dry were coverslipped using Dako mounting medium (Agilent Technologies, Santa Clara, CA). Slides were allowed to dry overnight in the dark. Tissue sections were imaged using a Zeiss LSM 710 confocal microscope. Utilizing Zen software (Zeiss), z-stacks (slice thickness 1 μm) were taken at various magnifications. All tissue was imaged using the same settings.

2.6 Statistical analyses

All data are presented as means ± standard error of the mean (SEM). The analyses were conducted in Statistical Package for the Social Sciences (SPSS v. 23; IBM) and Graphpad Prism (version 6; La Jolla, CA). Two-way ANOVAs were utilized for cell uptake work followed by Student's *t*-test with p less than 0.05 used as the criterion for significance. For *in vivo* work, two-way ANOVAs were conducted to analyze the effects of time (1, 4, 24 hours) and dendrimer type (D-Cy5; Mannose-D-Cy5) on uptake in various organs and serum. Post-hoc analyzes between treatments groups at various timepoints were conducted using unpaired *t*-tests. All *a priori* tests utilized a p value of 0.05. All post-hoc *t*-tests utilized a Bonferroni-corrected p value of 0.0167 to correct the alpha level to account for multiple comparisons. In figures * signifies $p < 0.05$, ** $p < 0.01$, and *** $p < 0.001$.

3. Results and discussion

3.1 Synthesis and physicochemical characterization of mannose receptor targeted fluorescently labeled hydroxyl PAMAM dendrimer conjugate (Mannose-D-Cy5)

To compare brain uptake and retention as well as overall biodistribution of mannosylated dendrimer with non-targeted dendrimer (D4-OH without any targeting ligand), mannose was modified and appended on the surface of D4-OH followed by the attachment of an imaging agent, Cy5, as a fluorescent tag. Initially, this dendrimer having 64 terminal hydroxyl groups is monofunctional, and, to introduce both targeting and imaging modalities, the surface of the dendrimer was modified to have multiple functions, which could participate in different chemical transformations independent of each other. Since conjugation reactions on macromolecules are often hampered by interactions with other functional moieties present, the chemical transformations for attachment of the ligands were carefully chosen to be highly selective and specific and to not interfere with the dendrimer surface itself. Mannose-conjugated fluorescent dendrimer was synthesized using a highly efficient and versatile CuAAC click chemistry[46] in combination with Steglich reaction[47]. The preparation of Mannose-D-Cy5 involved three main steps: 1) attachment of an orthogonal linker with azide terminal on mannose molecule (Fig. 1A), 2) synthesis of trifunctional dendrimer containing hydroxyl, acetylene, and amine functional groups (Fig. 1B), and 3) conjugation of mannose and Cy5 to construct the final conjugate (Fig. 1C). Details of the synthesis are described below:

3.1.1 Synthesis of azide-terminated triethylene glycol (TEG) conjugated mannose (5)—Mannose was modified to attach a TEG linker with azido focal point to participate in click reaction (Fig. 1A). The purpose of attachment of TEG linker is to provide flexibility to the targeting ligand for easy access to the receptors on the cell surface. The

synthesis of mannose-TEG-azide (**5**) began with peracetylation of commercially available D-(+)-mannose using acetic anhydride and pyridine to protect the hydroxyl groups. Monotosyl TEG was attached *via* boron trifluoride etherate ($BF_3{\cdot}Et_2O$) promoted glycosylation reaction to yield compound **3** with tosyl end-group. The tosylate function was further converted into an azido derivative **4** using sodium azide in DMF. The proton NMR clearly revealed the disappearance of tosyl signals in the aromatic region. Finally, the peracetate **4** was treated under typical Zemplén conditions (NaOMe–MeOH) to obtain completely de-*O*-acetylated mannose-TEG-N_3 (**5**) with a 90% yield. The completion of the reaction was confirmed by ^{1}H-NMR showing the complete disappearance of four distinct signals of acetyl protons from 2.16-1.99 ppm (SI). HRMS mass spectrometry also confirmed the formation of product showing mass peak corresponding to the sodium adduct (SI).

3.1.2 Synthesis of trifunctional dendrimer (8)—The surface of monofunctional D4-OH was modified to have two additional functions (5-6 alkynes and 1-2 amines) for appending additional ligands; a targeting agent, mannose; and an imaging dye, Cy5 (Fig. 1B). Only 10% (6-8 groups) of the hydroxyl surface groups of the dendrimer were modified to largely retain the inherent physico-chemical properties of the dendrimer. Chemical reactions were selected that could sustain the presence of a variety of functional groups, did not cause non-specific interactions and cross-reactivity with other functional moieties, and were highly efficient. We chose CuAAC click reaction based on its unique features such as high reaction yields, minimum side products, easy purification, and tolerance to a variety of solvents and functional groups. The synthesis of a trifunctional dendrimer started from commercially available D4-OH. An esterification reaction was carried out with 4-pentynoic acid using EDC/DMAP in DMF to obtain dendrimer **6** with acetylenes on the surface. ^{1}H NMR revealed the attachment of 5-6 alkyne linkers by comparing the integration of peaks for internal amide protons of dendrimer in between 7-8 ppm with methylene protons which show a clear shift at 4.02 ppm upon esterification (Fig. 2A). HPLC also confirmed the formation of product showing a shift in retention time from 22.4 min for D4-OH to 21.9 min for D4-pentyne (Fig. 2B). Subsequent esterification was carried out on dendrimer **6** with BOC-GABA-OH to attach 1-2 linkers with BOC protected amine on dendrimer **7**. ^{1}H NMR depicted the appearance of BOC protons at 1.3 ppm (Fig. S11). BOC groups in **7** were deprotected using trifluoroacetic acid (TFA) and the product as a TFA salt was treated with ion exchange resin to obtain trifunctional dendrimer **8** with 5-6 pentynes, 1-2 amines and 56-58 hydroxyl groups on the surface.

3.1.3 Synthesis of Mannose-D-Cy5 (10)—The trifunctional dendrimer **8** was utilized to attach the targeting ligand, mannose; and imaging dye, Cy5 (Fig. 1C). Mannose was clicked on the dendrimer first, followed by Cy5 due to the possibility of degradation of Cy5 under different chemical environments. The alkyne functions in dendrimer **8** were used to participate in click reaction with azido terminating mannose (**5**) under classical click conditions using copper sulfate and sodium ascorbate. ^{1}H NMR confirmed the formation of product revealing mannose protons and triazole protons (Fig. 2A). In addition, HPLC further confirmed the product formation showing a clear shift in the retention time (22.4 min, Fig. 2B). Finally, the amine groups in dendrimer **9** were reacted with Cy5 NHS ester to attach Cy5 at the surface of the dendrimer through amide linkages to yield dendrimer **10**. ^{1}H NMR

depicted the appearance of signals of Cy5; and HPLC revealed the absence of any impurities in the final conjugate with a shift in retention time from 22.6 to 23.3 minutes (Fig. 2A and B). The imaging dye was attached through amide bond so that it would not cleave *in vivo* and remain intact to study the biodistribution of the dendrimer. The size and zeta potential of the conjugate were measured and found to be similar to D4-OH (Fig. 2C and Table 1). It is important to maintain the size and surface charge of the targeted conjugate close to the non-targeted D4-OH to keep other parameters similar while evaluating the effect of mannose conjugation on brain uptake.

3.2 Effects of the competitive binding of mannan and cell activation on uptake of D-Cy5 and Mannose-D-Cy5

To investigate the ability of mannosylation to modify dendrimer biodistribution on a cellular level, we performed multiple *in vitro* assays utilizing RAW 264.7 murine macrophages, which have been shown to express CD206 in culture.[48] We initially performed experiments with LPS treatment at 100 ng/mL to induce an active phagocytic phenotype predominantly consisting of 'pro-inflammatory' M1 state macrophages to maintain continuity between the cell studies and the animal model.[49] Cells were also treated with exogenous mannan at 100 μg/mL to saturate mannose receptors,[50–52] a combination of LPS and mannan treatments, or left untreated. D-Cy5 and Mannose-D-Cy5 were then applied to separate wells with each treatment in duplicate, after which cells were recovered, counted, lysed, and analyzed for Cy5 fluorescent content. Cells exposed to the same culture conditions, but in the absence of dendrimer were also employed to identify the levels of CD206 expression with mannan or LPS treatments through RT-qPCR.

The application of LPS to the culture system was meant to simulate the inflammatory microenvironment in the brains of rabbit kits with CP, which results in increased levels of TNFα, decreased levels of IL1β, and other cytokine changes also observed in CP kits.[53] Under these conditions, CD206 expression had yet to be analyzed by our group, but RT-qPCR results indicate that with either LPS or mannan treatments there is no significant change in CD206 expression in RAW 264.7 murine macrophages (Fig. 3A) (Student's one-tailed *t*-test, $p>0.1$, n=4). RAW 264.7 cells do express a baseline level of CD206, and mannose receptor-mediated endocytosis is a cell entry pathway that has been implicated previously in dendrimer transport[54], so we performed a competitive uptake assay to observe any effects of dendrimer mannosylation on cellular internalization with and without the competitive binding of mannan to CD206.

We observed that mannan pre/co-treatment resulted in a significant decrease in dendrimer uptake for Mannose-D-Cy5 compared to D-Cy5 in LPS-activated cells (Student's paired two-tailed *t*-test, $p<0.05$, n=6) (Fig. 3B). Mannose-D-Cy5 was present in cells at levels ~1.4 times higher than in untreated cells whereas D-Cy5 uptake in activated cells with mannan present represented a ~2.5 fold increase from uptake in untreated cells. Additionally, when non-activated macrophages were pre-treated and co-treated with mannan, there was a trend indicating a lower uptake of Mannose-D-Cy5 as compared to D-Cy5 (Student's paired two-tailed *t*-test, $p<0.1$, n=6). Resting macrophages treated with mannan showed D-Cy5 levels

~1.7 fold higher than levels in untreated cells, and Mannose-D-Cy5 levels were comparable to those of untreated cells, showing only a ~1.1 fold increase.

We also performed preliminary competitive uptake studies with a pre-treatment of 5 mg/mL of mannan[55] for 10 minutes in addition to co-treatment for 12 hours (data not shown), and while no significant differences were observed there was a trend indicating an increase in Mannose-D-Cy5 uptake in resting macrophages treated with this high dose of mannan, indicating that mannan itself could be an agonist of CD206. Human microglia have been shown to express mannose receptor *in vitro*,[56, 57] and these cells are implicated in many preclinical animal models of CNS disorders including glioblastoma[58–60] and traumatic brain injury[61, 62]. Therefore, these initial results with LPS-activated macrophages encouraged an investigation of the performance of mannosylated dendrimer in culture conditions where CD206 is overexpressed.

Identical culture conditions to the studies above were employed, but this time with exogenous IL-4 treatment replacing LPS treatment. IL-4 administered at a concentration of 20 ng/mL has been shown to increase mannose receptor expression previously in mouse microglial culture, but to confirm the effects of IL-4 on CD206 expression in these culture conditions with RAW 264.7 cells RT-qPCR was again performed on cells not receiving dendrimer treatment (Fig. 3C). Cells were lysed at the endpoint of the dendrimer uptake studies, i.e. after 15 hours of IL-4 exposure. Previous studies have shown that mannose receptor expression will vary over the course of treatment in BV-2 cells, so the levels of CD206 expression could differ over the course of the experiment.[63] However, we observed a significant difference in CD206 expression in RAW 264.7 cells following 15 hours of IL-4 treatment, expressing CD206 at levels almost 20 times higher than control cells (Student's one-tailed *t*-test, $p<0.05$, n=3). There was no significant effect of mannan treatment alone. Having confirmed that IL-4 treatment will help obtain CD206 overexpression, the competitive uptake studies were then redone with IL-4 activation replacing LPS activation.

Two-way ANOVA of the fluorescent content of the cell lysates indicated a main effect of dendrimer [$F(1,22) = 5.926$, $p < 0.05$] and treatment conditions [$F(3,22) = 3.969$, $p < 0.05$], which then identified a significant increase in Mannose-D-Cy5 uptake compared to D-Cy5 uptake in the case of IL-4 treatment in the absence of mannan (Student's two-tailed t-test, $p<0.05$, n=3). When cells were treated with IL-4 and not mannan for competitive binding, Mannose-D-Cy5 entered cells at levels ~2.4 times higher than control cells whereas D-Cy5 only was present at levels ~1.1 times that of control cells. There was no significant change in D-Cy5 uptake between the treatment conditions. Additionally, in both cases where mannan was introduced to culture to competitively bind to CD206, Mannose-D-Cy5 uptake levels were not significantly different from D-Cy5 levels (Student's two-tailed *t*-test, $p>0.1$, n=3). The effects seen through fluorescence spectroscopy and RT-qPCR were confirmed through confocal microscopy of cells exposed to all four culture conditions and both types of dendrimer (Fig. 3E). These images clearly show that IL-4 increases the expression of CD206 in RAW 264.7 culture, as well as the heightened uptake of dendrimer when IL-4 treated cells were exposed to Mannose-D-Cy5.

The fact that only Mannose-D-Cy5 demonstrated an increase in cellular internalization with IL-4 treatments indicates that the treatment does not necessarily cause the cells to increase their phagocytic behavior. However, the increased uptake of mannosylated dendrimer in the case where CD206 is overexpressed and no mannan is introduced to competitively bind with the ligand indicates that Mannose-D-Cy5 uptake is more highly regulated by mannose receptor than unmodified dendrimer. When mannan is introduced to cells overexpressing CD206, Mannose-D-Cy5 uptake drops to baseline levels, which could be explained if the dendrimer can still employ the other methods of cell entry it has been known to utilize.[54, 64] These data seem to indicate that the conjugation of mannose to the dendrimer surface gives it an enhanced ability to target mannose receptors, while not impeding the dendrimer's natural ability to employ other fluid-phase endocytic routes of entry into the cell. This could then give mannosylated dendrimer an advantage at internalizing in CD206 expressing macrophages and microglia.

3.3 Comparative biodistribution of Mannose-D-Cy5 and D-Cy5 in a neonatal rabbit model of cerebral palsy

3.3.1 Tissue collection and brain microdissection for dendrimer quantification and confocal microscopy—Much of our previous work has been dedicated to the analysis of the effects of D4-OH in this CP model,[18, 19, 43, 65] and through this study the goal is to advance that work by performing the most detailed analysis yet of the biodistribution on both an organ and cellular scale. This began with the sacrifice of kits at 1, 4, and 24 hours after injection to investigate the retention and removal of dendrimer throughout the body over time (Fig. 4A). Brains were micro-dissected for 3 subregions – cortex, hippocampus, and periventricular region, through microdissection to enable a more detailed understanding of local dendrimer biodistribution within the brain (Fig. 4B). This is a modification of our group's previous methods, which either treated the brain as one organ or only analyzed dendrimer concentration in a few specific regions.[19, 22, 66] The advantage of microdissection is that it allows the evaluation of how the dendrimer is partitioning within the brain and if it is actually arriving at areas of clinical importance for the disease model under investigation. The regions were chosen for their importance in the cerebral palsy model. Generally, in this model activated microglia are observed in the periventricular region, white matter, and the hippocampus.[18] We analyzed uptake in the cortex as it is presumed to be less involved in this model and would allow for a relative comparison of the dendrimer uptake.

In addition to overall organ (and suborgan) dendrimer uptake, areas of interest were investigated at a cellular level out of concern for the specific types of cells the dendrimer was entering. What we found was majorly in congruence with our group's previous results that dendrimer mostly targets activated macrophages and microglia within the brain[67], but we also found dendrimer in non-macrophage cells. In the liver dendrimer was observed in cells that did not stain positive as either Kupffer cells or hepatocytes (data not shown), leading us to believe that they were residing in sinusoidal endothelial cells. While this begins to paint a more detailed picture, there is still much to be explored concerning the cellular biodistribution of dendrimer in many organs, which could lead to novel applications of the dendrimers for delivering therapies to not only activated microglia and macrophages.

3.3.2 Mannose conjugation did not affect the dendrimer uptake and cellular localization in the injured brain—D-Cy5 and Mannose-D-Cy5 uptake within the brain were evaluated quantitatively and qualitatively. When quantifying uptake of both dendrimer conjugates, the PVR, hippocampus and cortex were measured individually as described above. These analyses demonstrated that the conjugation of mannose to the dendrimer did not alter delivery to the brain (Fig. 4C). Across all regions of the brain that were analyzed through microdissection followed by fluorescence spectroscopy, there were no significant differences (for treatment $p>0.2$ in all three regions) between the uptake of Mannose-D-Cy5 and D-Cy5. Based on previous results we expect to extract about 1 μg of dendrimer per gram of tissue in the brain.[65] While this is possibly true for a whole-organ average, we saw that in the hippocampus dendrimer reached concentrations of about 2 μg per gram of tissue. Additionally the PVR expressed dendrimer concentrations at over 3 μg of dendrimer per gram of tissue, which is almost double the levels found in cortex. With similar levels across all subregions and time points, we believe that the conjugation of mannose impedes neither D4-OH's movement into the injured brain nor uptake by activated microglia/macrophages. The increased removal of Mannose-D-Cy5 over time as compared to D-Cy5 could be explained by the local biodistribution in the brain based on the cells Mannose-D-Cy5 targets or the decreased plasma levels resulting in lower Mannose-D-Cy5 concentration in the PVR over time. Regardless this result is not concerning as there was still enough dendrimer present to be clinically relevant throughout the regions analyzed[19] and there was no statistically significant difference between Mannose-D-Cy5 and D-Cy5 levels in the cortex and hippocampus.

In this rabbit model of cerebral palsy, we consistently see dendrimer uptake in white matter and the PVR of the neonatal brain as these have the most concentrated populations of activated microglia.[18, 22] Thus, we examined the PVR in rabbit kits injected with Mannose-D-Cy5 and D-Cy5 using fluorescent confocal microscopy. Fixed and preserved brain sections were stained for the identification of microglia/macrophages (Iba1) and mannose receptor (MR), and then imaged on a confocal microscope. We see similar patterns of uptake throughout this region. Both Mannose-D-Cy5 and D-Cy5 are present in the choroid plexus within the lateral ventricle, around the lateral ventricle in the periventricular region (Fig. 5). These microglia/macrophages that we are able to target using dendrimers are most likely of a pro-inflammatory phenotype as in these regions we see increased levels of TNFα and IL-6,[68] both pro-inflammatory cytokines. This suggests that the conjugation of mannose does not negatively impact the uptake of dendrimer into already preferred cells.

This model of cerebral palsy is generally indicated as a model of chronic pro-inflammatory response; however, mannose receptor is down-regulated in pro-inflammatory states and up-regulated in anti-inflammatory states[69] which suggests that we must look elsewhere within the brain of these endotoxin-exposed kits to determine if the conjugation of mannose alters uptake of dendrimer in MR+ cells. Thus we decided to look at a cell population with increased mannose receptor density. The meninges (the protective outer covering of the brain) have a high concentration of mannose receptor-positive microglia and macrophages. [25, 70] When looking at meningeal Iba1+ cells, we see a high proportion of MR colocalization. Both Mannose-D-Cy5 and D-Cy5 are readily taken up into MR+ microglia/

macrophages (Fig. 6). This suggests that the addition of Mannose to D4-OH does not alter the rate of uptake in cells that express MR in this model of cerebral palsy.

3.3.3 Conjugation of mannose alters the biodistribution of PAMAM dendrimers in major organs—The relative levels of non-targeted dendrimer in the major organs in this study is in broad agreement with previous work published by our group as well as other work on the biodistribution of PAMAM dendrimers.[19, 71–74] Quantitative analysis of the internal biodistribution demonstrated a significantly different localization of the dendrimers when a few (5-6) molecules of mannose were conjugated to the surface (Fig. 7). There was a significant increase in overall Mannose-D-Cy5 uptake as compared to D-Cy5 uptake in the liver ($F(1,35)=64.362$, $p<0.001$, $e^2=0.648$), plasma ($F(1,34)=8.224$, $p<0.01$, $e^2=0.195$), spleen ($F(1,33)=8.509$, $p<0.01$, $e^2=0.205$), and heart ($F(1,35)=6.844$, $p<0.05$, $e^2=0.164$). Mannose-D-Cy5 accumulates higher in the liver, which contains 3.55% of the injected dose of dendrimer within an hour and increases to 8.59% by 24 hours. Unmodified D-Cy5 has a much lower concentration in the liver with a maximum uptake of 1.35% of the injected dose at 4 hours after injection. This indicates that conjugating just a few molecules of mannose to the dendrimer changed how the dendrimer interacts with different cells, showing a preference for uptake in the liver when normally D4-OH is cleared through the kidney.[67] Mannose receptor-expressing cells exist in high quantities in the liver,[75, 76] of which sinusoidal endothelial cells (SECs) are a significant population and have been shown to highly express MR.[77] In confocal imaging of liver slices from rabbits injected with Mannose-D-Cy5 (data not shown), the cells with Mannose-D-Cy5 uptake did not stain for Kupffer cell or hepatocyte markers, indicating their likelihood of being SECs. This further shows that the conjugation of mannose to the dendrimer surface modified how dendrimers bind to cell surfaces and are taken up, significantly increasing the dendrimer's preference for uptake by MR expressing cells, through most likely mannose receptor-mediated endocytosis. Serum levels for Mannose-D-Cy5 were also significantly lower than D-Cy5 over time, starting at just 1.8 fold lower and becoming over 11 fold lower by 24 hours. The rapid removal of Mannose-D-Cy5 is probably due in a large part to the accumulation of Mannose-D-Cy5 in the liver, giving insight into the delicate balance between dendrimer circulation and clearance.

These findings demonstrate that while the addition of mannose significantly alters overall biodistribution of G4 PAMAM dendrimers, it does not meaningfully affect uptake to microglia and macrophages in this model of cerebral palsy. In the rabbit CP model, there was not an appreciable increase in the mannose-receptor on glia, upon injury. However, it may be that in a disease model with more anti-inflammatory processes and mannose receptor involvement there may be an enhanced uptake and microglia localization of Mannose-D-Cy5 within the CNS. Moreover, the conjugation of other targeting ligands could allow these dendrimers to be tailored to treat a variety of inflammatory diseases, not limited to just the CNS disorders for which they are being investigated today.[21–23, 37, 78]

4. Conclusions

We have demonstrated an efficient and facile synthetic approach based on highly robust and orthogonal CuAAC click reaction to modify the surface of PAMAM hydroxyl-terminated

dendrimers from monofunctional to trifunctional having a combination of hydroxyl, alkyne and amine functionalities. The trifunctional dendrimer developed here is a potential platform to conjugate a combination of variety of therapeutic molecules, fluorescent dyes and targeting agents, potentially allowing simultaneous, targeted imaging and treatment of a disease. We successfully conjugated both mannose and Cy5 on the dendrimer surface to study the effect of mannose conjugation on the biodistribution of hydroxyl PAMAM dendrimer. Our results suggest that the conjugation of targeting ligand to the dendrimer surface drastically impacts the way that cells interact with dendrimers, as the conjugation of mannose to the dendrimer increased its preference for uptake through mannose receptor-mediated endocytosis. The conjugation of mannose to the dendrimer revealed that targeting ligands have appreciable potential in this field, demonstrating an ability to alter how generation 4 hydroxyl-terminated PAMAM dendrimers interact with individual cells throughout the body while not diminishing the dendrimers' inherent targeting of neuroinflammation. The presence of CD206 expression in this CP model seems to be lower than previously thought as there were no changes in brain uptake with the addition of mannose to the dendrimer although we did observe a more global change in biodistribution. Further investigation of these findings leads us to believe that the addition of mannose for enhanced dendrimer targeting would be most beneficial in conditions in which CD206 is enhanced greatly as in glioblastoma. Dendrimers have already been shown to be adept at targeting neuroinflammation within the brain, but with the advent of trifunctional dendrimers and the proof that targeting can modify biodistribution and cell-dendrimer interactions, the potential for dendrimer application in theranostics only continues to expand.

Supplementary Material

Refer to Web version on PubMed Central for supplementary material.

Acknowledgments

This study was funded by the NIBIB R01EB018306 (RM Kannan). We acknowledge Jinhuan Liu and Dr. Elena Zhang for rabbit breeding and surgeries. We also acknowledge the Wilmer core facility and imaging center (core grant: P30EY001765) for confocal microscopy facilities.

Abbreviations

CNS	central nervous system
BBB	blood-brain barrier
D4-OH	generation four PAMAM dendrimers
CuAAC	Cu(I)-catalyzed alkyne–azide cycloaddition
Cy5	cyanine 5 dye
CP	cerebral palsy
CD	cluster of differentiation
PAMAM	polyamidoamine

EDC	*N*-(3-Dimethylaminopropyl)-*N*′-ethylcarbodiimide hydrochloride
DMAP	4-(dimethylamino)pyridine
DIPEA	*NN*′-diisopropylethylamine
TFA	trifluoroacetic acid
BOC-GABA-OH	γ-(Boc-amino)butyric acid
DCM	dichloromethane
THF	tetrahydrofuran
DMF	dimethylformamide
NMR	Nuclear Magnetic Resonance
MALDI	Matrix-assisted laser desorption/ionization
SECs	sinusoidal endothelial cells

References

1. Wohlfart S, Gelperina S, Kreuter J. Transport of drugs across the blood–brain barrier by nanoparticles. J Control Release. 2012; 161:264–273. [PubMed: 21872624]
2. Pardridge WM. The Blood-Brain Barrier: Bottleneck in Brain Drug Development. NeuroRx. 2005; 2:3–14. [PubMed: 15717053]
3. Barchet TM, Amiji MM. Challenges and opportunities in CNS delivery of therapeutics for neurodegenerative diseases. Expert Opin Drug Deliv. 2009; 6:211–225. [PubMed: 19290842]
4. Ekta K, Viral S, Kalpesh B. Drug Delivery to CNS: Challenges and Opportunities with Emphasis on Biomaterials Based Drug Delivery Strategies. Curr Pharm Des. 2016; 22:2913–2922. [PubMed: 27033697]
5. Kannan RM, Nance E, Kannan S, Tomalia DA. Emerging concepts in dendrimer-based nanomedicine: from design principles to clinical applications. J Intern Med. 2014; 276:579–617. [PubMed: 24995512]
6. Mignani S, Bryszewska M, Zablocka M, Klajnert-Maculewicz B, Cladera J, Shcharbin D, Majoral JP. Can dendrimer based nanoparticles fight neurodegenerative diseases? Current situation versus other established approaches. Prog Polym Sci. 2017; 64:23–51.
7. Zhang F, Lin YA, Kannan S, Kannan RM. Targeting specific cells in the brain with nanomedicines for CNS therapies. J Control Release. 2016; 240:212–226. [PubMed: 26686078]
8. Caminade AM, Turrin CO. Dendrimers for drug delivery. J Mater Chem B. 2014; 2:4055–4066.
9. Mintzer MA, Grinstaff MW. Biomedical applications of dendrimers: a tutorial. Chem Soc Rev. 2011; 40:173–190. [PubMed: 20877875]
10. Sharma A, Mejia D, Maysinger D, Kakkar A. Design and synthesis of multifunctional traceable dendrimers for visualizing drug delivery. RSC Adv. 2014; 4:19242–19245.
11. Tomalia DA, Reyna LA, Svenson S. Dendrimers as multi-purpose nanodevices for oncology drug delivery and diagnostic imaging. Biochem Soc Trans. 2007; 35:61–67. [PubMed: 17233602]
12. Mignani S, Bryszewska M, Zablocka M, Klajnert-Maculewicz B, Cladera J, Shcharbin D, Majoral JP. Can dendrimer based nanoparticles fight neurodegenerative diseases? Current situation versus other established approaches. Prog Polym Sci. 2017; 64:23–51.
13. Esfand R, Tomalia DA. Poly(amidoamine) (PAMAM) dendrimers: from biomimicry to drug delivery and biomedical applications. Drug Des Discov. 2001; 6:427–436.

14. Kim SH, Madak-Erdogan Z, Bae SC, Carlson KE, Mayne CG, Granick S, Katzenellenbogen BS, Katzenellenbogen JA. Ligand Accessibility and Bioactivity of a Hormone–Dendrimer Conjugate Depend on pH and pH History. Journal of the American Chemical Society. 2015; 137:10326–10335. [PubMed: 26186415]
15. Ohyama A, Higashi T, Motoyama K, Arima H. In Vitro and In Vivo Tumor-Targeting siRNA Delivery Using Folate-PEG-appended Dendrimer (G4)/α-Cyclodextrin Conjugates. Bioconjugate Chemistry. 2016; 27:521–532. [PubMed: 26715308]
16. Zhou Z, Wang Y, Yan Y, Zhang Q, Cheng Y. Dendrimer-Templated Ultrasmall and Multifunctional Photothermal Agents for Efficient Tumor Ablation. ACS Nano. 2016; 10:4863–4872. [PubMed: 27054555]
17. Marina AD. Dendrimers Effects on the Immune System: Insights into Toxicity and Therapeutic Utility. Current Pharmaceutical Design. 2017; 23:1–8. [PubMed: 28292246]
18. Kannan S, Dai H, Navath RS, Balakrishnan B, Jyoti A, Janisse J, Romero R, Kannan RM. Dendrimer-Based Postnatal Therapy for Neuroinflammation and Cerebral Palsy in a Rabbit Model. Sci Transl Med. 2012; 4:130ra146–130ra146.
19. Lesniak WG, Mishra MK, Jyoti A, Balakrishnan B, Zhang F, Nance E, Romero R, Kannan S, Kannan RM. Biodistribution of Fluorescently Labeled PAMAM Dendrimers in Neonatal Rabbits: Effect of Neuroinflammation. Mol Pharm. 2013; 10:4560–4571. [PubMed: 24116950]
20. Dai H, Navath RS, Balakrishnan B, Guru BR, Mishra MK, Romero R, Kannan RM, Kannan S. Intrinsic targeting of inflammatory cells in the brain by polyamidoamine dendrimers upon subarachnoid administration. Nanomedicine (London, England). 2010; 5:1317–1329.
21. Kambhampati SP, Clunies-Ross AJM, Bhutto I, Mishra MK, Edwards M, McLeod DS, Kannan RM, Lutty G. Systemic and Intravitreal Delivery of Dendrimers to Activated Microglia/Macrophage in Ischemia/Reperfusion Mouse RetinaRetinal Microglia Uptake of Dendrimers. Invest Ophthalmol Vis Sci. 2015; 56:4413–4424. [PubMed: 26193917]
22. Nance E, Porambo M, Zhang F, Mishra MK, Buelow M, Getzenberg R, Johnston M, Kannan RM, Fatemi A, Kannan S. Systemic dendrimer-drug treatment of ischemia-induced neonatal white matter injury. J Control Release. 2015; 214:112–120. [PubMed: 26184052]
23. Mishra MK, Beaty CA, Lesniak WG, Kambhampati SP, Zhang F, Wilson MA, Blue ME, Troncoso JC, Kannan S, Johnston MV, Baumgartner WA, Kannan RM. Dendrimer Brain Uptake and Targeted Therapy for Brain Injury in a Large Animal Model of Hypothermic Circulatory Arrest. ACS Nano. 2014; 8:2134–2147. [PubMed: 24499315]
24. Guo Y, Johnson MA, Mehrabian Z, Mishra MK, Kannan R, Miller NR, Bernstein SL. Dendrimers Target the Ischemic Lesion in Rodent and Primate Models of Nonarteritic Anterior Ischemic Optic Neuropathy. PLOS ONE. 2016; 11:e0154437. [PubMed: 27128315]
25. Burudi EME, Régnier-Vigouroux A. Regional and cellular expression of the mannose receptor in the post-natal developing mouse brain. Cell and Tissue Research. 2001; 303:307–317. [PubMed: 11320646]
26. Marzolo MP, von Bernhardi R, Inestrosa NC. Mannose receptor is present in a functional state in rat microglial cells. J Neurosci Res. 1999; 58:387–395. [PubMed: 10518112]
27. Varin A, Gordon S. Alternative activation of macrophages: Immune function and cellular biology. Immunobiology. 2009; 214:630–641. [PubMed: 19264378]
28. Tietze C, Schlesinger P, Stahl P. Mannose-specific endocytosis receptor of alveolar macrophages: demonstration of two functionally distinct intracellular pools of receptor and their roles in receptor recycling. J Cell Biol. 1982; 92:417–424. [PubMed: 6277962]
29. Kruskal BA, Sastry K, Warner AB, Mathieu CE, Ezekowitz RA. Phagocytic chimeric receptors require both transmembrane and cytoplasmic domains from the mannose receptor. J Exp Med. 1992; 176:1673–1680. [PubMed: 1460425]
30. Sung S, Nelson R, Silverstein S. Yeast Mannans inhibit binding and phagocytosis of zymosan by mouse peritoneal macrophages. J Cell Biol. 1983; 96:160–166. [PubMed: 6298248]
31. Woller EK, Cloninger MJ. Mannose Functionalization of a Sixth Generation Dendrimer. Biomacromolecules. 2001; 2:1052–1054. [PubMed: 11710009]

32. Sharma A, Khatchadourian A, Khanna K, Sharma R, Kakkar A, Maysinger D. Multivalent niacin nanoconjugates for delivery to cytoplasmic lipid droplets. Biomaterials. 2011; 32:1419–1429. [PubMed: 21071082]
33. Sharma R, Zhang I, Shiao TC, Pavan GM, Maysinger D, Roy R. Low generation polyamine dendrimers bearing flexible tetraethylene glycol as nanocarriers for plasmids and siRNA. Nanoscale. 2016; 8:5106–5119. [PubMed: 26868181]
34. Tang W, Becker ML. "Click" reactions: a versatile toolbox for the synthesis of peptide-conjugates. Chem Soc Rev. 2014; 43:7013–7039. [PubMed: 24993161]
35. Neibert K, Gosein V, Sharma A, Khan M, Whitehead MA, Maysinger D, Kakkar A. "Click" Dendrimers as Anti-inflammatory Agents: With Insights into Their Binding from Molecular Modeling Studies. Mol Pharm. 2013; 10:2502–2508. [PubMed: 23590185]
36. Sharma A, Mejía D, Regnaud A, Uhlig N, Li CJ, Maysinger D, Kakkar A. Combined A3 Coupling and Click Chemistry Approach for the Synthesis of Dendrimer-Based Biological Tools. ACS Macro Lett. 2014; 3:1079–1083.
37. Sharma R, Zhang I, Abbassi L, Rej R, Maysinger D, Roy R. A fast track strategy toward highly functionalized dendrimers with different structural layers: an "onion peel approach". Polym Chem. 2015; 6:1436–1444.
38. Wu P, Malkoch M, Hunt JN, Vestberg R, Kaltgrad E, Finn MG, Fokin VV, Sharpless KB, Hawker CJ. Multivalent, bifunctional dendrimers prepared by click chemistry. Chem Commun. 2005:5775–5777.
39. Sharma A, Neibert K, Sharma R, Hourani R, Maysinger D, Kakkar A. Facile Construction of Multifunctional Nanocarriers Using Sequential Click Chemistry for Applications in Biology. Macromolecules. 2011; 44:521–529.
40. Franc G, Kakkar A. Dendrimer design using CuI-catalyzed alkyne-azide "click-chemistry". Chem Commun. 2008:5267–5276.
41. Manzo E, Ciavatta ML, Pagano D, Fontana A. An efficient and versatile chemical synthesis of bioactive glyco-glycerolipids. Tetrahedron Lett. 2012; 53:879–881.
42. Liaw K, Gök O, DeRidder LB, Kannan S, Kannan RM. Quantitative assessment of surface functionality effects on microglial uptake and retention of PAMAM dendrimers. Journal of Nanoparticle Research. 2018; 20:111.
43. Zhang F, Nance E, Alnasser Y, Kannan R, Kannan S. Microglial migration and interactions with dendrimer nanoparticles are altered in the presence of neuroinflammation. Journal of Neuroinflammation. 2016; 13:65. [PubMed: 27004516]
44. Kannan S, Saadani-Makki F, Muzik O, Chakraborty P, Mangner TJ, Janisse J, Romero R, Chugani DC. Microglial Activation in Perinatal Rabbit Brain Induced by Intrauterine Inflammation: Detection with 11C-(R)-PK11195 and Small-Animal PET. J Nucl Med. 2007; 48:946–954. [PubMed: 17504871]
45. Balakrishnan B, Dai H, Janisse J, Romero R, Kannan S. Maternal Endotoxin Exposure Results in Abnormal Neuronal Architecture in the Newborn Rabbit. Dev Neurosci. 2013; 35:396–405. [PubMed: 23988854]
46. Rostovtsev VV, Green LG, Fokin VV, Sharpless KB. A Stepwise Huisgen Cycloaddition Process: Copper(I)-Catalyzed Regioselective "Ligation" of Azides and Terminal Alkynes. Angew Chem Int Ed. 2002; 41:2596–2599.
47. Neises B, Steglich W. Simple Method for the Esterification of Carboxylic Acids. Angew Chem Int Ed. 1978; 17:522–524.
48. Phan TA, Taylor AW. The neuropeptides α-MSH and NPY modulate phagocytosis and phagolysosome activation in RAW 264.7 cells. J Neuroimmunol. 2013; 260:9–16. [PubMed: 23689030]
49. Navath RS, Kurtoglu YE, Wang B, Kannan S, Romero R, Kannan RM. Dendrimer–Drug Conjugates for Tailored Intracellular Drug Release Based on Glutathione Levels. Bioconjugate Chem. 2008; 19:2446–2455.
50. Gennari A, Pelliccia M, Donno R, Kimber I, Tirelli N. Mannosylation Allows for Synergic (CD44/C-Type Lectin) Uptake of Hyaluronic Acid Nanoparticles in Dendritic Cells, but Only upon Correct Ligand Presentation. Adv Healthcare Mater. 2016; 5:966–976.

51. Minami SS, Sun B, Popat K, Kauppinen T, Pleiss M, Zhou Y, Ward ME, Floreancig P, Mucke L, Desai T, Gan L. Selective targeting of microglia by quantum dots. J Neuroinflammation. 2012; 9:22. [PubMed: 22272874]
52. Gallud A, Bondarenko O, Feliu N, Kupferschmidt N, Atluri R, Garcia-Bennett A, Fadeel B. Macrophage activation status determines the internalization of mesoporous silica particles of different sizes: Exploring the role of different pattern recognition receptors. Biomaterials. 2017; 121:28–40. [PubMed: 28063981]
53. Zhang Z, Jyoti A, Balakrishnan B, Williams M, Singh S, Chugani DC, Kannan S. Trajectory of inflammatory and microglial activation markers in the postnatal rabbit brain following intrauterine endotoxin exposure. Neurobiol Dis. 2018; 111:153–162. [PubMed: 29274431]
54. Perumal OP, Inapagolla R, Kannan S, Kannan RM. The effect of surface functionality on cellular trafficking of dendrimers. Biomaterials. 2008; 29:3469–3476. [PubMed: 18501424]
55. Gennari A, Pelliccia M, Donno R, Kimber I, Tirelli N. Mannosylation Allows for Synergic (CD44/C-Type Lectin) Uptake of Hyaluronic Acid Nanoparticles in Dendritic Cells, but Only upon Correct Ligand Presentation. Adv Healthcare Mater. 2016; 5:966–976.
56. Stahl PD, Ezekowitz RAB. The mannose receptor is a pattern recognition receptor involved in host defense. Curr Opin Immunol. 1998; 10:50–55. [PubMed: 9523111]
57. Durafourt BA, Moore CS, Zammit DA, Johnson TA, Zaguia F, Guiot MC, Bar-Or A, Antel JP. Comparison of polarization properties of human adult microglia and blood-derived macrophages. Glia. 2012; 60:717–727. [PubMed: 22290798]
58. Li W, Graeber MB. The molecular profile of microglia under the influence of glioma. Neuro-Oncology. 2012; 14:958–978. [PubMed: 22573310]
59. Komohara Y, Ohnishi K, Kuratsu J, Takeya M. Possible involvement of the M2 anti-inflammatory macrophage phenotype in growth of human gliomas. J Pathol. 2008; 216:15–24. [PubMed: 18553315]
60. Hambardzumyan D, Gutmann DH, Kettenmann H. The role of microglia and macrophages in glioma maintenance and progression. Nat Neurosci. 2016; 19:20–27. [PubMed: 26713745]
61. Hsieh CL, Kim CC, Ryba BE, Niemi EC, Bando JK, Locksley RM, Liu J, Nakamura MC, Seaman WE. Traumatic brain injury induces macrophage subsets in the brain. Eur J Immunol. 2013; 43:2010–2022. [PubMed: 23630120]
62. Wang G, Zhang J, Hu X, Zhang L, Mao L, Jiang X, Liou AKF, Leak RK, Gao Y, Chen J. Microglia/Macrophage Polarization Dynamics in White Matter after Traumatic Brain Injury. J Cereb Blood Flow Metab. 2013; 33:1864–1874. [PubMed: 23942366]
63. Latta CH, Sudduth TL, Weekman EM, Brothers HM, Abner EL, Popa GJ, Mendenhall MD, Gonzalez-Oregon F, Braun K, Wilcock DM. Determining the role of IL-4 induced neuroinflammation in microglial activity and amyloid-β in V microglial cells and APP/PS1 transgenic mice. Journal of Neuroinflammation. 2015; 12:41. [PubMed: 25885682]
64. Liaw K, Gök O, DeRidder LB, Kannan S, Kannan RM. Quantitative assessment of surface functionality effects on microglial uptake and retention of PAMAM dendrimers. J Nanopart Res. 2018; 20:111.
65. Nance E, Zhang F, Mishra MK, Zhang Z, Kambhampati SP, Kannan RM, Kannan S. Nanoscale effects in dendrimer-mediated targeting of neuroinflammation. Biomaterials. 2016; 101:96–107. [PubMed: 27267631]
66. Zhang F, Trent Magruder J, Lin Y-A, Crawford TC, Grimm JC, Sciortino CM, Wilson MA, Blue ME, Kannan S, Johnston MV, Baumgartner WA, Kannan RM. Generation-6 hydroxyl PAMAM dendrimers improve CNS penetration from intravenous administration in a large animal brain injury model. J Control Release. 2017; 249:173–182. [PubMed: 28137632]
67. Lesniak WG, Mishra MK, Jyoti A, Balakrishnan B, Zhang F, Nance E. Biodistribution of fluorescently labeled PAMAM dendrimers in neonatal rabbits: effect of neuroinflammation. Mol Pharm. 2013; 10
68. Zhang F, Nance E, Zhang Z, Jasty V, Kambhampati SP, Mishra MK, Burd I, Romero R, Kannan S, Kannan RM. Surface functionality affects the biodistribution and microglia-targeting of intra-amniotically delivered dendrimers. J Control Release. 2016; 237:61–70. [PubMed: 27378700]

69. Régnier-Vigouroux A. Int Rev Cytol. Academic Press; 2003. The Mannose Receptor in the Brain; 321–342.

70. Galea I, Palin K, Newman TA, Van Rooijen N, Perry VH, Boche D. Mannose receptor expression specifically reveals perivascular macrophages in normal, injured, and diseased mouse brain. Glia. 2005; 49:375–384. [PubMed: 15538754]

71. Khan MK, Nigavekar SS, Minc LD, Kariapper MST, Nair BM, Lesniak WG, Balogh LP. In Vivo Biodistribution of Dendrimers and Dendrimer Nanocomposites — Implications for Cancer Imaging and Therapy. Technol Cancer Res Treat. 2005; 4:603–613. [PubMed: 16292880]

72. Sadekar S, Ray A, Janàt-Amsbury M, Peterson CM, Ghandehari H. Comparative Biodistribution of PAMAM Dendrimers and HPMA Copolymers in Ovarian-Tumor-Bearing Mice. Biomacromolecules. 2011; 12:88–96. [PubMed: 21128624]

73. Nigavekar SS, Sung LY, Llanes M, El-Jawahri A, Lawrence TS, Becker CW, Balogh L, Khan MK. 3H Dendrimer Nanoparticle Organ/Tumor Distribution. Pharm Res. 2004; 21:476–483. [PubMed: 15070099]

74. Kojima C, Regino C, Umeda Y, Kobayashi H, Kono K. Influence of dendrimer generation and polyethylene glycol length on the biodistribution of PEGylated dendrimers. Int J Pharm. 2010; 383:293–296. [PubMed: 19761822]

75. Linehan SA, Martínez-Pomares L, Stahl PD, Gordon S. Mannose Receptor and Its Putative Ligands in Normal Murine Lymphoid and Nonlymphoid Organs: In Situ Expression of Mannose Receptor by Selected Macrophages, Endothelial Cells, Perivascular Microglia, and Mesangial Cells, but not Dendritic Cells. J Exp Med. 1999; 189:1961–1972. [PubMed: 10377192]

76. Lee SH, Starkey PM, Gordon S. Quantitative analysis of total macrophage content in adult mouse tissues. Immunochemical studies with monoclonal antibody F4/80. J Exp Med. 1985; 161:475–489. [PubMed: 3973536]

77. Magnússon S, Berg T. Endocytosis of ricin by rat liver cells in vivo and in vitro is mainly mediated by mannose receptors on sinusoidal endothelial cells. Biochem J. 1993; 291:749–755. [PubMed: 8489503]

78. Mastorakos P, Kambhampati SP, Mishra MK, Wu T, Song E, Hanes J, Kannan RM. Hydroxyl PAMAM dendrimer-based gene vectors for transgene delivery to human retinal pigment epithelial cells(). Nanoscale. 2015; 7:3845–3856. [PubMed: 25213606]

Highlights

- Trifunctional PAMAM dendrimer was constructed using CuAAC click chemistry
- Both mannose and Cy5 were conjugated to the dendrimer surface
- Dendrimer with mannose utilizes mannose receptor-mediated endocytosis
- Mannosylated dendrimer resides in mannose receptor positive cells in vivo
- Mannose conjugation did not reduce uptake of dendrimer in the brain

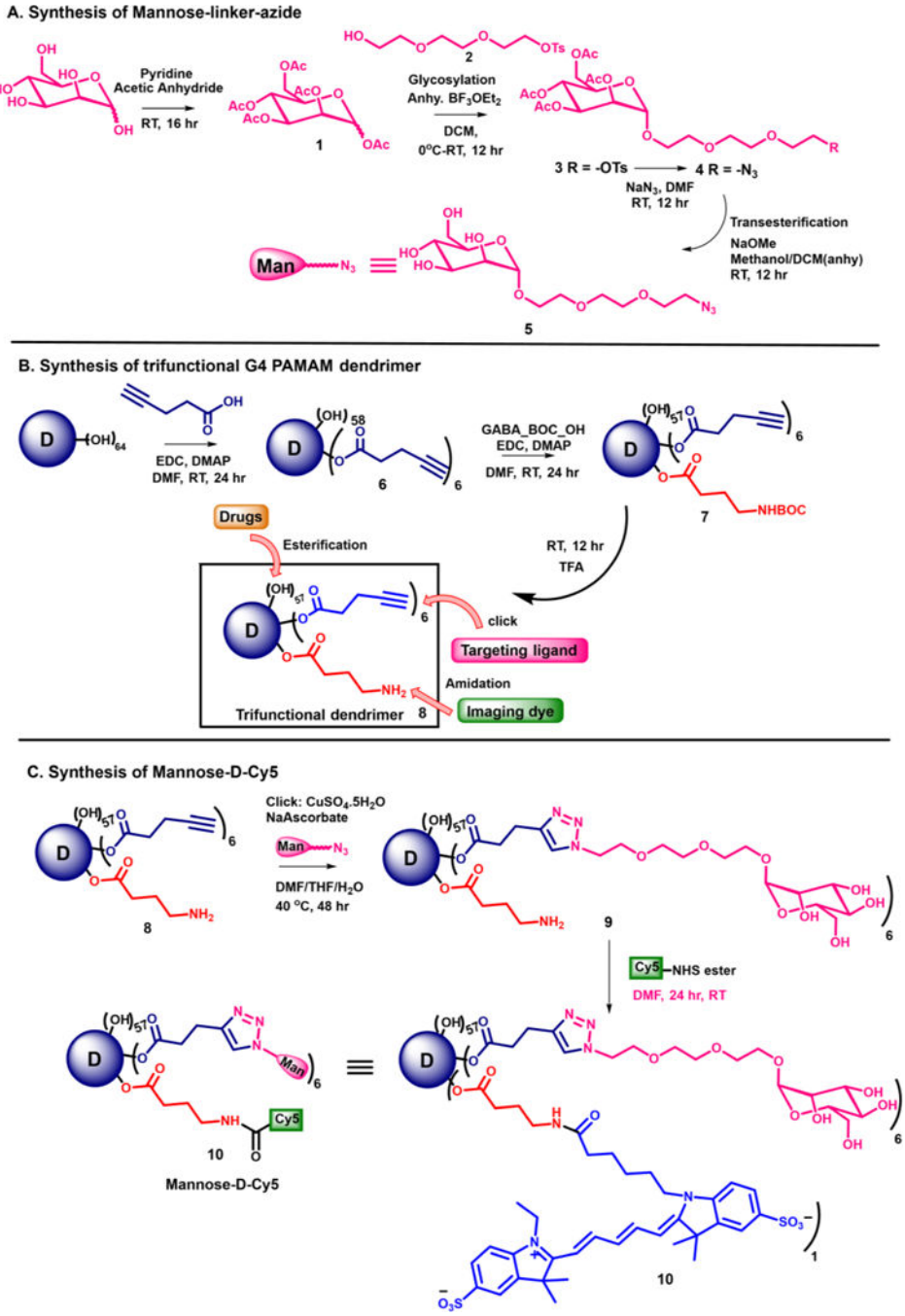

Figure 1.

(A) Schematic representation of synthesis of azide-terminated mannose linker (**5**). **(B)** Synthetic approach to trifunctional dendrimer (**8**) having a combination of alkyne, amine and hydroxyl functional groups which can independently participate in CuAAC click, amidation, and Steglich esterification reactions to selectively conjugate targeting ligands, imaging dye, and/or therapeutic molecules respectively. **(C)** Synthetic route to the synthesis of targeted dendrimer Mannose-D-Cy5 (**10**) having mannose as targeting ligands and Cy5 as an imaging agent.

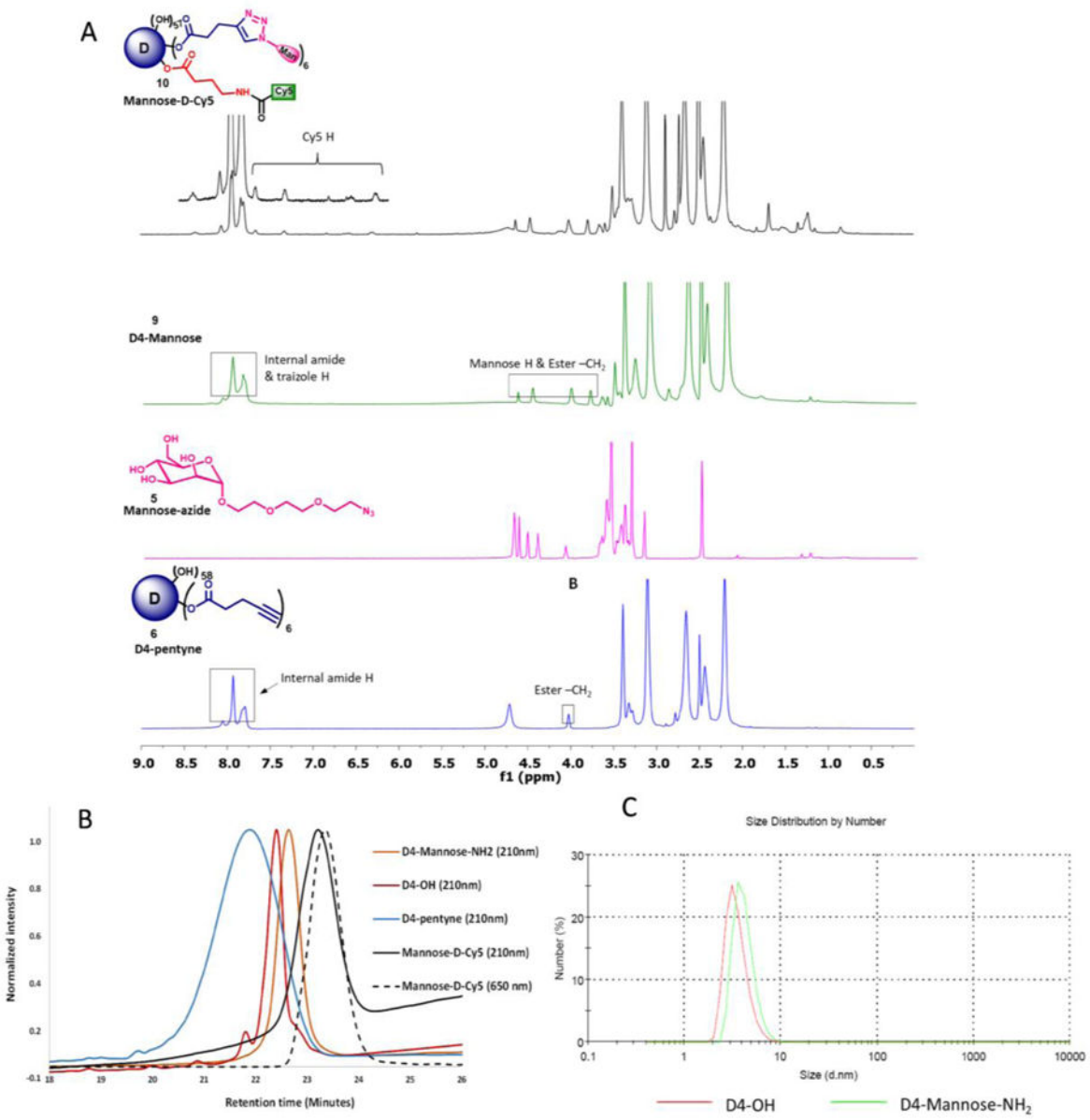

Figure 2.

(A) Comparison of ^{1}H NMR spectra (DMSO, 500 MHz) of D4-Pentyne (**6**), Mannose azide (**5**), D4-Mannose (**9**), and Mannose-D-Cy5 (**10**) showing the appearance or disappearance of characteristic signals. **(B)** The HPLC chromatogram of the starting dendrimer (D4-OH), intermediates (D4-pentyne, D4-mannose-NH_2), and final conjugate (Mannose-D-Cy5) confirming the purity and successful conjugation of mannose and Cy5. Each intermediate shows a clear shift in retention time; **D4-OH** (22.4 min), **D4-pentyne** (21.8 min), **D4-Mannose-NH_2** (22.6 min) and **Mannose-D-Cy5** (23.3 min). All peaks were monitored at λ=210 nm. Mannose-D-Cy5 was also monitored at λ=650 nm (dashed line). **(C)** Comparison of size distribution of both targeted (D4-OH) and non-targeted (D4-Mannose-NH_2) dendrimer using dynamic light scattering. Both the starting dendrimer and mannose conjugated dendrimer have similar size. Conjugation of 6 molecules of mannose did not

significantly alter the size of the dendrimer. The zeta potential of mannose conjugated dendrimer was close to neutral.

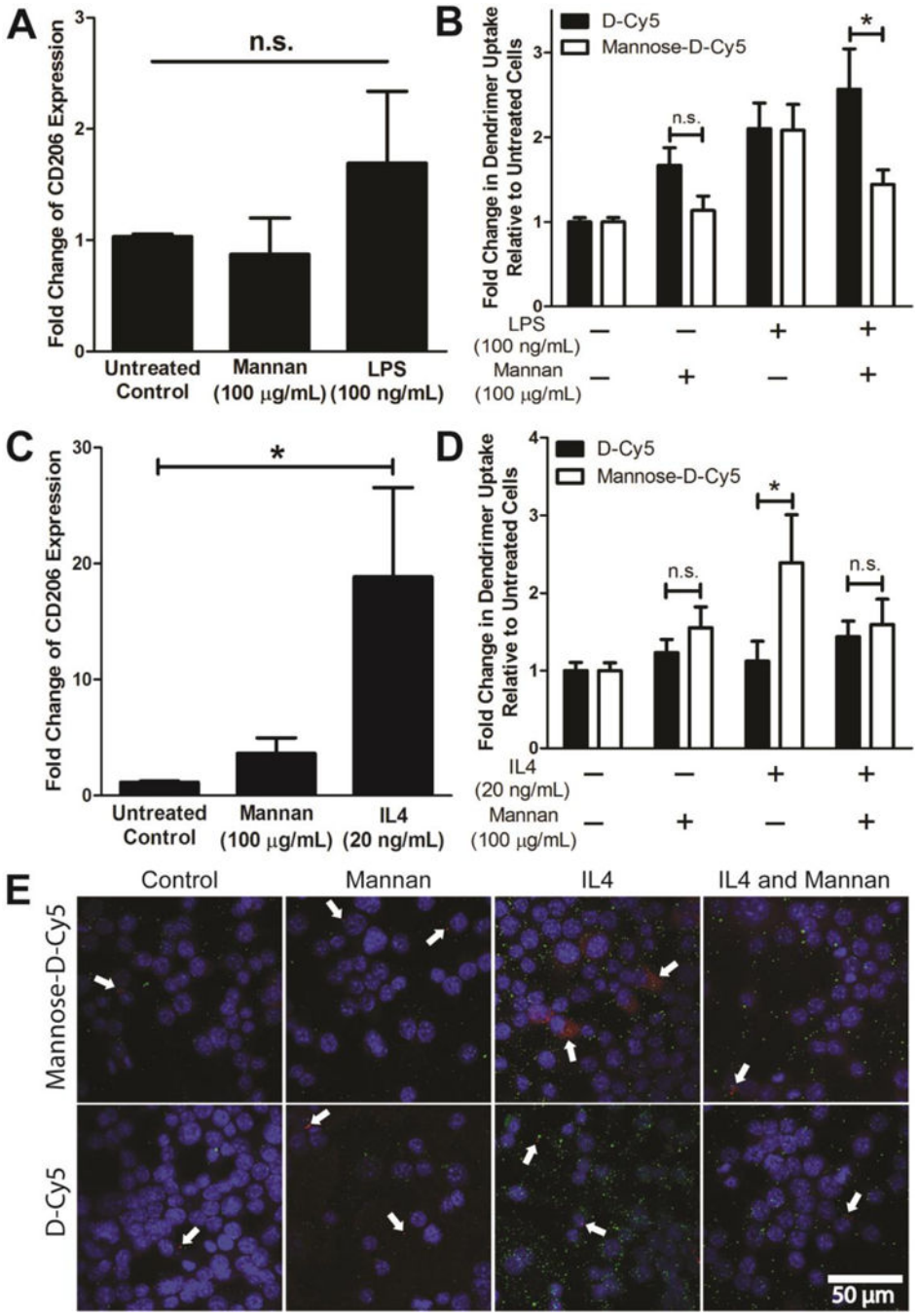

Figure 3.

Cells were treated with LPS to activate, mannan to block mannose receptor, both, or neither. **A.** RT-qPCR for CD206 expression of LPS and mannan treated cells. (n=4) **B.** Dendrimer internalization of cells given the previously stated treatments. (n=6). The same treatment scheme was then replicated with IL-4 replacing LPS. **C.** RT-qPCR for CD206 expression of IL-4 and mannan treated cells. (n=3) **D.** Internalized dendrimer content of cells undergoing IL-4 and mannan treatments. (n=3) **E.** Representative confocal microscopy images of cells

undergoing the same treatments as **D**, showing expression of CD206 (green) and localization of dendrimer (red) within the cells. Nuclei are stained with DAPI and shown in blue.

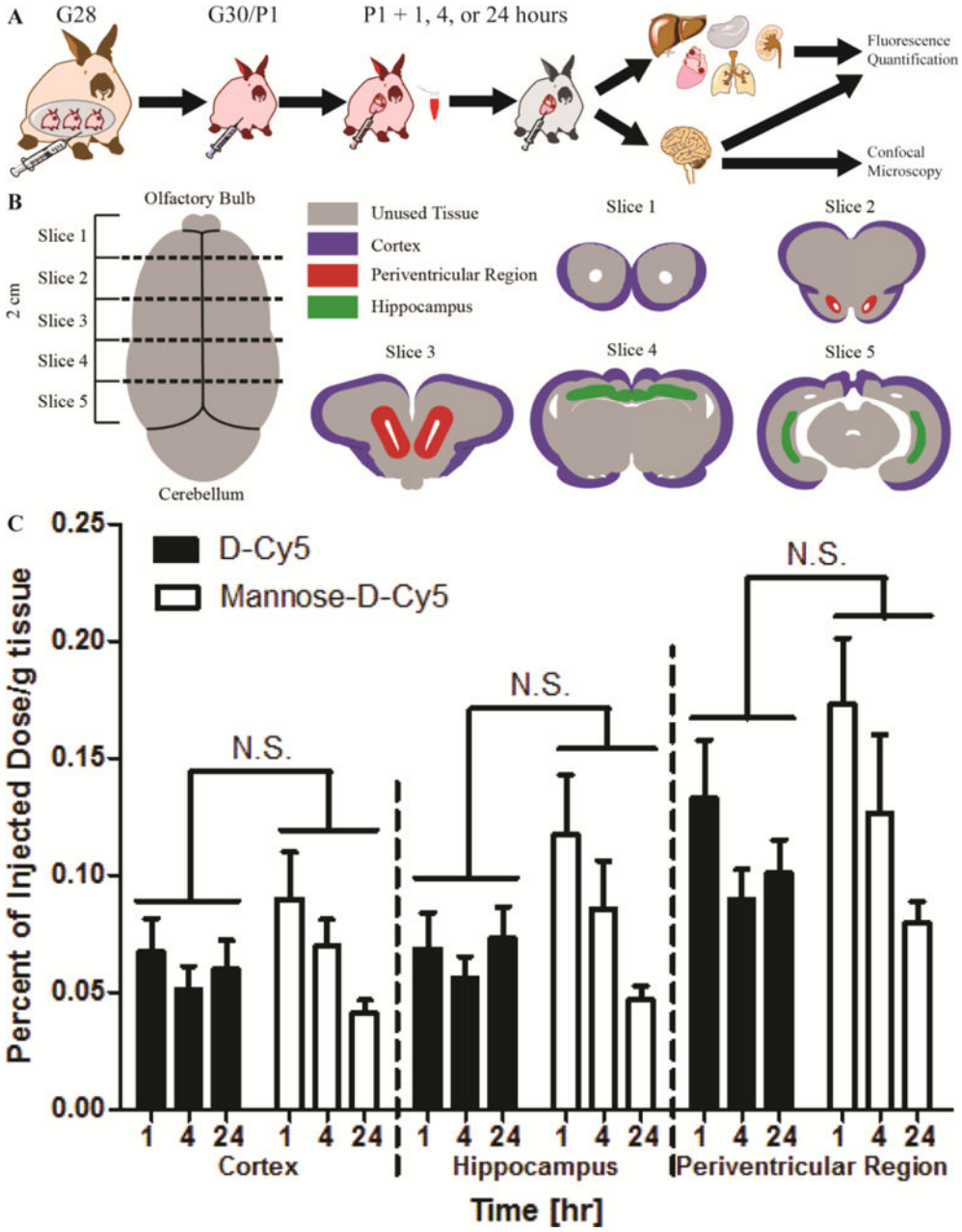

Figure 4.

(A) Experimental design for the modeling cerebral palsy in rabbit kits, treatment with dendrimer, and isolation of the blood, brain, and internal organs for fluorescence quantification and confocal microscopy. **(B)** Procedure for the microdissection of the coronal brain sections of CP neonatal rabbit kits for isolation of cortex, hippocampus, and periventricular region. The regions that were isolated and quantified for dendrimer biodistribution in each brain are as follows: cortex (blue), hippocampus (green), and periventricular region (red). All tissue on which biodistribution analysis was not performed is labeled in gray. **(C)** Quantitative comparative biodistribution of Mannose-D-Cy5 and D-

Cy5 in neonatal rabbit kits with cerebral palsy in three subregions of the brain over time points of 1, 4, and 24 hours (n=6).

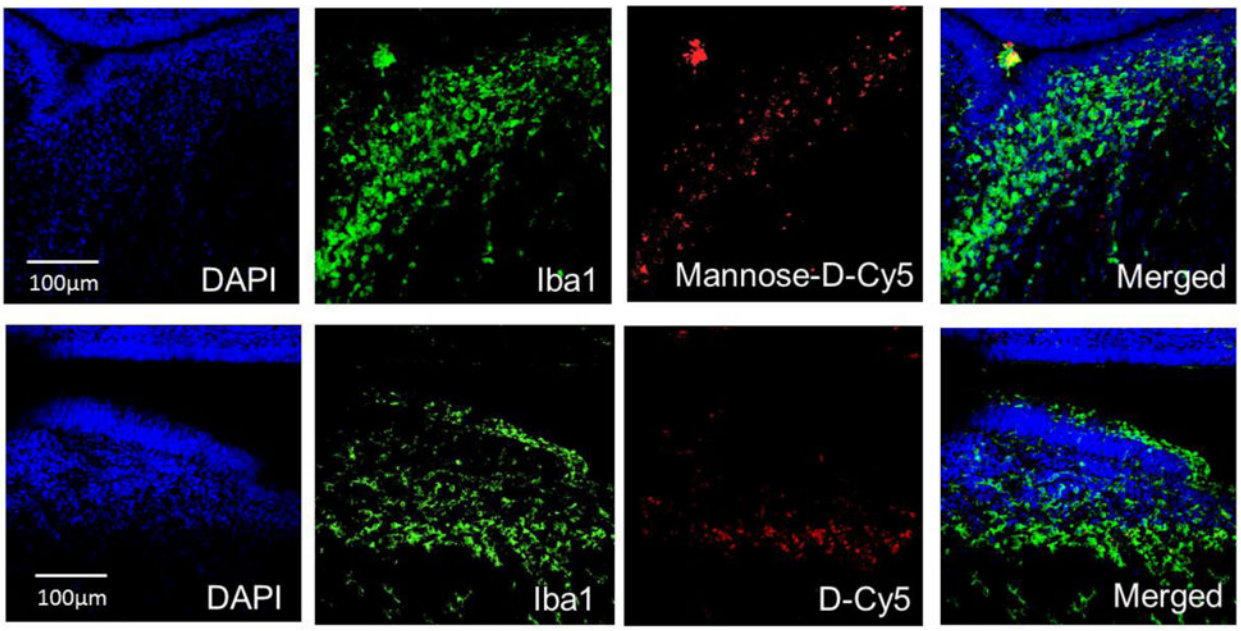

Figure 5.

Confocal microscopy of dendrimer uptake in the PVR of P1 rabbit kits 24 hours post-injection. Immunohistochemical staining was conducted to label all cell bodies (DAPI; blue), microglia (Iba1; green) to determine if D-Cy5 or Mannose-D-Cy5 (both magenta) were being taken into microglia. D-Cy5 is generally seen in the periventricular region (PVR) both within the ventricle and in the surrounding gray matter in this model of cerebral palsy. Mannose-D-Cy5 is also found in a similar pattern both within the ventricle in the choroid plexus and in the cell bodies surrounding the ventricle.

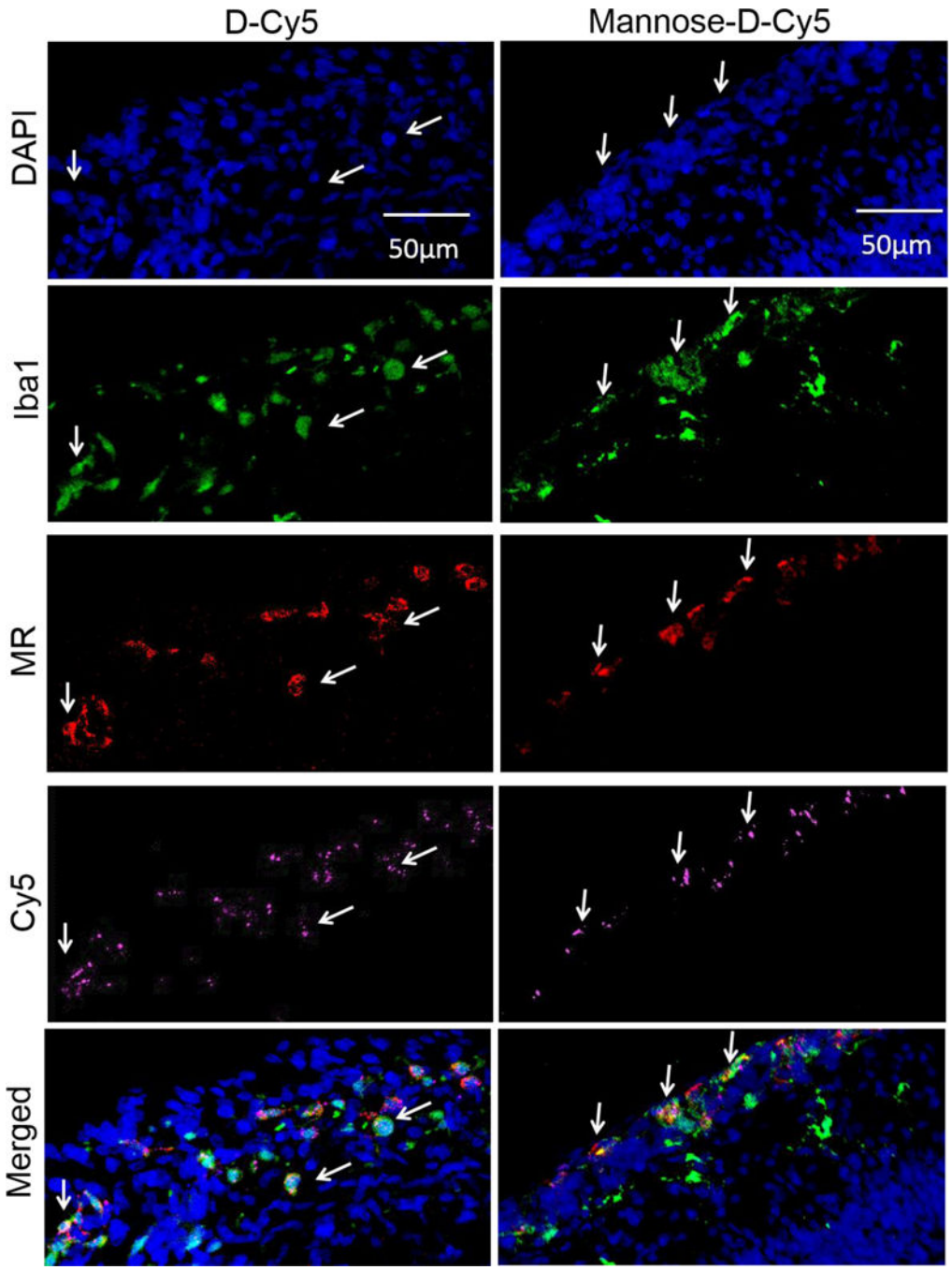

Figure 6.

Colocalization of Cy5 signal in mannose receptor positive (MR+) microglia/macrophages within the meninges 24 hours post-injection. To determine if dendrimer uptake was altered by mannose addition, microglia/macrophages (Iba1; green) were co-stained for mannose receptor were tagged (MR, red). MR is found in high density within the meninges. Upon examination it seems both D-Cy5 and Mannose-D-Cy5 (magenta) show uptake in MR/Iba1 double-positive cells (white arrows).

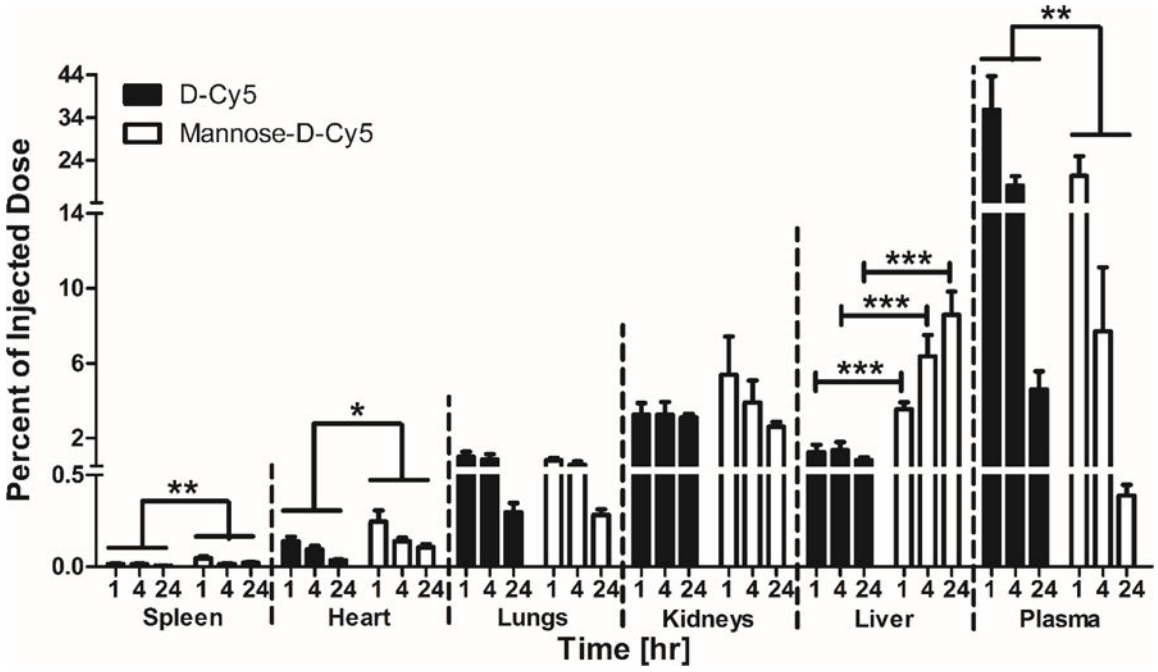

Figure 7.

Quantitative comparative biodistribution of Mannose-D-Cy5 and D-Cy5 in the major organs and blood plasma of neonatal rabbit kits with cerebral palsy over time points of 1, 4, and 24 hours. Results are reported in terms of percent of the injected dose found in the total organ (or plasma volume) (n=6).

Table 1

Dynamic light scattering (DLS) and Zeta potential (ζ) measurements of D4-OH and D4-Mannose-NH_2 (Compound **9**):

Sample	Theoretical M Wt. (g/mole)	Size (nm)	Zeta potential (ζ, mV)
D4-OH	14, 279	4.4±0.2	4.5 ± 0.6
D4-Mannose-NH_2 (Compound 10)	16,978	4.2±0.1	2.0±0.5
Mannose-D-Cy5 * (Compound 10)	17,583	–	–

* The size and ζ-potential of Mannose-D-Cy5 was not measured through dynamic light scattering due to the high absorbance of Cy5. Both non-targeted (D4-OH) and targeted (D4-Mannose-NH_2) dendrimers have similar size and neutral charge.